A genome-wide CRIPR-Cas9 screen identifies TGN46 as a host determinant for H-1PV susceptibility in pancreatic adenocarcinoma.

Guillaume Labrousse[1,2], Nina Suarez[1,2], Adèle Nevot[1,2], Naïma Hanoun[1,2], Nelson Dusetti[3], Louis Buscail[1,4], Claudio Murgia[2,5] and Pierre Cordelier[1,2,4,#].

1 : Univ Toulouse, CNRS, INSERM, CRCT, Toulouse, France. Equipe labellisée Fondation ARC.

2 : member of the ImCORE network.

3: Aix Marseille Univ, CNRS, INSERM, Institut Paoli-Calmettes, CRCM, Marseille, France

4: Department of Gastroenterology and Pancreatology, Toulouse-Rangueil University Hospital (CHU), Toulouse, France.

5: Building 5, Roche Pharma Research and Early Development (pRED), Roche Innovation Center, Basel, Switzerland.

*: corresponding author

Pierre Cordelier, Cancer Research Center of Toulouse (CRCT)

Team: “Therapeutic innovation in pancreatic cancer”

2, avenue Hubert Curien, 31100 Toulouse, France.

Email: pierre.cordelier@inserm.fr

Tel: +33(0)582741641

Abstract

Pancreatic ductal adenocarcinoma (PDAC) remains a highly lethal malignancy with limited response to current therapeutic strategies. Oncolytic viruses such as the rat protoparvovirus H-1PV represent promising alternatives; however, their clinical development is hindered by an incomplete understanding of virus-host interactions that determine tumor susceptibility. Here, we conducted a genome-scale CRISPR-Cas9 knockout screen in primary PDAC cultures to identify host determinants of viral infection and cytotoxicity. The screen confirmed the central role of the sialylation pathway in mediating susceptibility to H-1PV and uncovered several additional genes involved in vesicular trafficking and protein recycling. Among these candidates, *TGOLN2*, encoding the transmembrane protein TGN46, emerged as a critical host factor. Functional analyses demonstrate that TGN46 supports efficient H-1PV infection, replication, and virus-induced cytotoxicity in pancreatic cancer cells. TGN46 colocalizes with viral particles at the cell surface and facilitates their internalization through dynamin-dependent endocytosis. Molecular studies further indicate that the luminal N-terminal domain of TGN46 interacts with the viral capsid. *In vivo*, *TGOLN2* expression in essential to H-1PV-mediated antitumor activity in experimental models. Collectively, these findings identify TGN46 as a membrane-associated entry factor required for optimal H-1PV infection in PDAC cells. This work refines the mechanistic understanding of H-1PV tropism and provides a rationale for exploring host determinants of viral susceptibility as candidate biomarkers to guide parvovirus-based virotherapy.

Introduction

Pancreatic adenocarcinoma (PDAC) is notoriously resistant to therapy and difficult to cure, with a 5-year survival rate of patients less than 11%[1,2]. This poor prognosis is primarily due to the limited efficacy of current treatments, despite recent advances[3]. Most existing options, primarily chemotherapies, have shown modest benefits. In contrast, oncolytic viruses (OVs) are emerging as a promising therapeutic alternative. OVs are naturally occurring or engineered viruses that selectively infect and kill cancer cells while sparing normal tissues. They replicate within tumor cells, causing direct oncolysis and releasing tumor antigens, which can stimulate systemic anti-tumor immunity[4]. Notable example is Talimogene laherparepvec (T-VEC), an engineered herpes simplex virus approved for melanoma treatment, which has demonstrated clinical efficacy[5]. Various OVs have been investigated in preclinical and clinical settings for their ability to target and eliminate PDAC cells[6]. However, the varying efficacy of OVs in PDAC including the limited success of T-VEC[7], highlights the critical need to understand the molecular and cellular mechanisms underlying oncolytic activity. In particular, identifying host factors in tumor cells may help refine patient selection and optimize therapeutic outcomes with virotherapy.

Among the OV strains currently under investigation for PDAC, the rat H-1 protoparvovirus (H-1PV) displays particularly promising properties. H-1PV is not a human pathogen and is not associated with any known human disease. It demonstrates natural tropism and strong oncolytic activity across various cancer cell types, both *in vitro* and *in vivo* [8]. Moreover, it is well-tolerated in patients, with no severe adverse effects directly attributed to the virus, in phase I/IIa and phase II clinical trials in glioblastoma [9] and PDAC [10,11]. These findings support the potential of H-1PV as a viable candidate for oncolytic virotherapy in PDAC. H-1PV is a small, 25 nm encapsidated virus that carries a 5 kb linear single-stranded DNA genome encoding four proteins from two genes. The early P4 promoter drives expression of the non-structural (NS) proteins NS1 and NS2. NS1 is essential for viral genome replication in the host cell nucleus and activates the late P38 promoter, which controls the expression of the viral capsid proteins VP1 and VP2. These capsid proteins assemble into new virions following viral DNA packaging[12]. The oncolytic activity of H-1PV primarily relies on NS1-induced production of reactive oxygen species (ROS) and subsequent cell death resulting from DNA damage[13].

Significant efforts have been made to better understand H-1PV and its interaction with host cells. An emerging model of H-1PV entry highlights the role of the laminin γ1 chain in anchoring viral particles to the extracellular matrix (ECM)[14]. Galectin-1 (Gal-1) is also implicated in this process, cooperating with laminin during viral entry, although it does not contribute to the initial attachment of viral particles to the cell surface[14,15]. Sialic acid (SIA) metabolism probably plays a central role in this mechanism, as H-1PV binding to laminin γ1 depends on specific SIA

79 glycosylation motifs. Galectins can further interact with sialylated proteins to modulate viral
80 infection, depending on the particular sialylation pattern[16]. Following attachment, H-1PV enters
81 cells via clathrin-mediated endocytosis (CME)[17], eventually escaping from the endosomal
82 compartment[18]. However, despite being discovered more than 60 years ago[19], a specific
83 cellular receptor for H-1PV has yet to be identified.

84 In this study, we aimed to identify novel host genes involved in H-1PV infection of PDAC cells,
85 with a particular focus on discovering candidates that may serve as potential viral receptors.
86 We performed a genome-scale CRISPR/Cas9 knockout (KO) screen in primary PDAC cultures
87 with intermediate sensitivity to viral infection and confirmed the essential role of the protein
88 sialylation pathway in H-1PV susceptibility. In parallel, we identified several host genes
89 associated with vesicular recycling, retrograde transport, and protein secretion. Among these,
90 we focused on *TGOLN2* (Trans-Golgi Network Protein 2), which encodes TGN46, a
91 glycosylated transmembrane protein that cycles rapidly between the cell surface and the trans-
92 Golgi network (TGN)[20]. We demonstrated that H-1PV critically depends on TGN46 for efficient
93 infection, replication, and cytotoxicity in primary PDAC cells. Further molecular analyses
94 indicate that TGN46 colocalizes with H-1PV at the cell surface and facilitates rapid viral
95 internalization in a dynamin-dependent manner. We also provide evidence that the N-terminal
96 luminal domain of TGN46 interacts with the H-1PV capsid, in a process influenced by
97 sialylation. Moreover, TGN46 expression associates with H-1PV permissiveness and
98 antitumor activity in pancreatic cancer models, both *in vitro* and *in vivo*. Together, these
99 findings identify TGN46 as a membrane-associated entry factor required for efficient H-1PV
100 infection and refine the current understanding of parvovirus tropism. This work establishes a
101 mechanistic basis for further exploration of host determinants as potential biomarkers of
102 response to parvovirus-based virotherapy.

103

Materials and Methods

Cell culture and treatment. HeLa S3 (ATCC CCL-2™), HEK-293T (ATCC CRL-3216™), and human newborn kidney cells NB-324K (kindly provided by Dr. Jean Rommelaere, DKFZ, Heidelberg, Germany) were cultured in Dulbecco's Modified Eagle Medium (DMEM, 4.5 g/L glucose; Sigma-Aldrich, D6429) supplemented with 10% fetal calf serum (FCS; Gibco, 10270-106) and 1× antibiotic-antimycotic solution (Gibco, 15240-062). Human primary pancreatic cancer cells were maintained as previously described[21]. All cells were cultured at 37°C in a humidified atmosphere containing 5% CO_2. Doxycycline (Dox; Sigma-Aldrich, D9891) was dissolved in PBS at a stock concentration of 0.5 mM and used at a final concentration of 0.5 µM. For inducible overexpression experiments, cells were pre-treated with doxycycline at least 24 hours before seeding and continuously exposed throughout the experiment. Dynasore (Tocris Bioscience, 2897), a dynamin inhibitor, was dissolved in DMSO at a stock concentration of 25 mM and used at a final concentration of 100 µM. Cells were pre-treated for 2 hours prior to experimentation and maintained under treatment during the assay. Transferrin from human serum conjugated to Alexa Fluor™ 647 (TFn-647; Fisher Scientific, 11550766) was reconstituted in deionized water at a stock concentration of 5 mg/mL and applied to cells at a final concentration of 25 µg/mL for 5 minutes prior to fixation. For antibiotic selection, blasticidin (InvivoGen, ant-bl) was used at 0.5 µg/mL, puromycin (InvivoGen, ant-pr) at 1 µg/mL, and ouabain (Sigma-Aldrich, O3125) at 0.5 µM. Selection was carried out for a minimum of one week.

Plasmid amplification and transfection. DNA plasmid constructs used in this study were transformed and amplified in E. coli Stbl3™ competent cells (Invitrogen - C7373-03). Bacteria were plated on LB agar supplemented with the appropriate antibiotic, and individual colonies were expanded for plasmid extraction. Initial plasmid preparations were performed using the ZR Plasmid Miniprep Classic kit (Zymo Research, D4016). Clones were verified by restriction enzyme digestion and Sanger sequencing (Eurofins Genomics, LightRun). For large-scale preparations, endotoxin-free plasmid DNA was obtained using the NucleoBond Xtra Maxi kit (Macherey-Nagel, 740414.50). At each step, plasmid DNA concentration and purity were assessed using a NanoDrop spectrophotometer (ND-1000, Thermo Scientific). Cell transfections were performed using JetPRIME transfection reagent (Polyplus, 101000046) according to the manufacturer's instructions, using a DNA:JetPRIME ratio of 1:2 (µg:µL).

Virus Production. The initial stock of H-1 protoparvovirus (H-1PV) was kindly provided by Dr. Jean Rommelaere (DKFZ, Heidelberg, Germany). For virus amplification, 1.5×10^6 NB-324K cells were seeded in T175 flasks and cultured until reaching approximately 30% confluency. Cells were then infected with H-1PV at a multiplicity of infection (MOI) of 10^{-2} in 3 mL of infection medium (IM) consisting of Opti-MEM (Gibco, 31985-047) supplemented with 1%

140 HEPES (Gibco, 15630-056) for 1 hour at 37 °C. After the adsorption period, the medium was
141 replaced with 20 mL of fresh Opti-MEM, and cells were incubated at 37 °C for 4 days until the
142 appearance of cytopathic effects (CPE). Cells were harvested by scraping into a minimal
143 volume of fresh Opti-MEM. Virions were released by three freeze–thaw cycles using liquid
144 nitrogen, followed by sonication on ice at 25 W for 30 seconds. Cellular debris were removed
145 by centrifugation at 1,800 rpm for 15 minutes, and the supernatant was filtered through a
146 0.2 µm membrane (ClearLine, 146560). Viral stocks were aliquoted and stored at −80 °C. Viral
147 titers were determined by plaque assay on NB-324K cells as previously described[22].

148 **Lentivirus production and cell transduction**. On day 1, for each lentiviral production, 4.5 ×
149 10^6 HEK-293T cells were seeded in a 100 mm dish with 10 mL of complete DMEM. On day 2,
150 HEK-293T cells were co-transfected with 6 µg of lentiviral plasmid, 4 µg of the psPAX2
151 packaging plasmid (Addgene #12260), and 1.5 µg of the pMD2.G envelope plasmid (Addgene
152 #12259) using JetPRIME reagent. Four hours post-transfection, the medium was replaced with
153 10 mL of Opti-MEM. On day 3, target cells were seeded in 6-well plates to reach 30–40%
154 confluency by the next day. On day 4, HEK-293T supernatants were collected in 50 mL tubes,
155 centrifuged for 5 minutes at 1800 rpm to remove cell debris, and the supernatant was filtered
156 through a 0.45 µm filter (Millex-HP, SLHP033RS). Lentiviral supernatants were concentrated
157 using Vivaspin 20 columns (100 kDa MWCO PES; Sartorius, VS2042) by centrifugation at
158 2500 rpm for 20–30 minutes. Target cells were transduced with the lentiviral vectors in 2 mL of
159 Opti-MEM supplemented with protamine sulfate at a final concentration of 10 µg/mL. Forty-
160 eight hours post-transduction, cells were expanded, and appropriate antibiotic selection was
161 initiated the following day. Selection was maintained for at least one week, and cells were
162 passaged at least twice before experimental use.

163 **CRISPR knock-out screen**. The CRISPR knock-out (KO) screen methodology was adapted
164 from[23]. Briefly, PDAC087T cells were first transduced with lentiCas9-Blast (Addgene #52962),
165 enabling constitutive expression of the Cas9 enzyme and resistance to blasticidin. After
166 antibiotic selection and expansion, PDAC087T-Cas9 cells were seeded in five T175 flasks at
167 1 × 10^7 cells per flask and transduced with the GeckoV2 pooled gRNA libraries A and B,
168 inserted in the lentiGuide-Puro plasmid (Addgene #1000000049), at a multiplicity of infection
169 (MOI) of ~0.3. This low MOI maximizes the probability of integrating a single sgRNA per cell
170 while maintaining library complexity. Following one week of puromycin selection, 7.5 × 10^6
171 PDAC087T-Cas9-GeckoV2 cells were seeded in seven T175 flasks per condition (>5 × 10^7
172 cells total). The following day, cells were incubated for 1 h at 37 °C with 5 mL infection medium
173 (IM), with or without H-1PV at MOI 10 (a dose previously shown to induce >90% cell death in
174 PDAC087T cells within 48 h). After infection, cells were washed with PBS and incubated in
175 20 mL of complete DMEM at 37 °C. Non-infected cells were passaged at a 1:10 dilution upon

176 reaching confluency. After one week, dead and floating cells were removed by repeated PBS
177 washes. Adherent cells from each condition were detached by trypsinization, centrifuged,
178 resuspended in complete medium, and pooled into one T175 flask per condition. Two days
179 later, cells were harvested again, resuspended in PBS, counted, and genomic DNA was
180 extracted using the DNeasy Blood & Tissue Kit (Qiagen #69504; one column per 5×10^6 cells,
181 with elution in minimal volume). For each condition, sgRNA loci were amplified using NGS-
182 grade barcoded PCR primers (Eurogentec, Table 1). Amplicons were size-separated by
183 electrophoresis on 2% agarose gel, purified with the NucleoSpin Gel and PCR Clean-up Kit
184 (Macherey-Nagel #740609.250), and further cleaned using SPRIselect Beads (Beckman
185 Coulter #B24965AA). DNA fragment size was monitored at each step using a Fragment
186 Analyzer (Agilent). Once quality was confirmed, barcoded amplicons were sequenced on the
187 NextSeq 550 platform (Illumina). Sequencing data were demultiplexed using the bcl2fastq
188 algorithm (Illumina) and analyzed for sgRNA enrichment using MAGeCK (Model-based
189 Analysis of Genome-wide CRISPR-Cas9 Knockout)[24].

190 **Generation of knock-out cell lines**. To generate knock-out (KO) cell lines for individual genes
191 of interest, sgRNA protospacer sequences targeting specific loci were ordered as
192 complementary oligonucleotides. Each oligo pair was phosphorylated using T4 Polynucleotide
193 Kinase (NEB #M0201) and annealed in a T100 Thermal Cycler (Bio-Rad #1861096) by heating
194 at 95 °C for 5 min, followed by a gradual temperature ramp down at 0.1 °C/sec to 25 °C.
195 Subcloning of the annealed protospacer sequences was performed by Golden Gate assembly.
196 Appropriate cohesive ends were designed to enable ligation of the protospacer DNA into either
197 the lentiGuide-Puro plasmid (Addgene #52963) or the eSpCas9 (1.1) No FLAG ATP1 A1G2
198 Dual sgRNA plasmid (Addgene #86612), previously digested with BsmBI (NEB #R0739) or
199 BbsI (NEB #R3539), respectively. For validation of sgRNAs identified in the CRISPR KO
200 screen, PDAC087T-Cas9 cells were thawed and seeded in 6-well plates at a density of $1.5 \times$
201 10^5 cells per well. The following day, each well was transduced with a different lentiGuide-Puro
202 construct carrying one sgRNA to validate. Cells were then selected with puromycin prior to
203 downstream use. The sequences of the sgRNAs used are listed in Table 2. To generate
204 *TGOLN2*-KO cells while avoiding constitutive expression of Cas9 and sgRNA, PDAC087T and
205 HeLa S3 cells were seeded in 6-well plates at 1.5×10^5 cells per well and transfected the
206 following day with 3 µg of the eSpCas9 (1.1) No FLAG ATP1A1 G2 Dual sgRNA plasmid. This
207 construct expresses Cas9 along with a sgRNA targeting exon 3 of *TGOLN2*. To enrich for
208 successfully edited cells, the plasmid also contains a second sgRNA targeting exon 4 of the
209 ATP1A1 gene, an essential gene whose disruption confers resistance to ouabain, a cytotoxic
210 drug. This strategy selectively enriches cells that have undergone mutagenic repair at the
211 ATP1A1 locus without impairing its function[25]. For generation of TGN46-WT control cells

212 undergoing the same transfection and selection process, a similar construct expressing only
213 the ATP1A1-targeting sgRNA was transfected in parallel. Five days post-transfection, ouabain
214 was added to the culture medium. After one week of recovery, *TGOLN2* KO efficiency was
215 assessed by Western blot and immunofluorescence.

216 ***TGOLN2* cDNA cloning**. Total mRNA from PDAC087T cells was extracted using the RNeasy
217 Plus Mini Kit (Qiagen #74134) and reverse-transcribed into complementary DNA (cDNA) with
218 the RevertAid Kit (Thermo Fisher #K1691). The resulting cDNA was used as a template for
219 high-fidelity PCR amplification of the open reading frame (ORF) corresponding to the main
220 *TGOLN2*-201 spliced variant (Ensembl transcript ID: ENST00000377386.8), which encodes
221 the 437-amino acid TGN46 protein (6050 bp). PCR amplification was performed using
222 PrimeSTAR Max DNA Polymerase (Takara #R045A). To facilitate downstream cloning, gene-
223 specific primers containing restriction sites were used: an AvrII site at the 5' end and a MluI
224 site at the 3' end. The sequences were as follows: Forward: 5′-
225 TTTACGCGTttaggacttctggtccaaac-3′, Reverse: 5′-TTTCCTAGGgccaccatgcggttcgtggttgcctt-3.
226 The PCR product was purified using the NucleoSpin Gel and PCR Clean-up Kit (Macherey-
227 Nagel), digested for 1 h at 37 °C with AvrII and MluI restriction enzymes (NEB #R3198,
228 #R0174), and re-purified before ligation into a similarly digested third-generation lentiviral
229 vector, pLIX402 (Addgene #41394), to generate the pTRE- *TGOLN2* construct. This all-in-one
230 plasmid contains the complete Tet-On system, including a constitutive expression cassette
231 encoding the rtTA-3 transactivator, followed by a 2A self-cleaving peptide and the puromycin
232 resistance gene. Upon doxycycline (dox) treatment, rtTA-3 binds to the TRE (tetracycline-
233 responsive element) promoter, thereby inducing the expression of TGN46.

234 ***TGOLN2* mutagenesis and fusion with EGFP and FLAG tags.** TGN46 deletion constructs,
235 TGN46-ΔI, TGN46-ΔII, and TGN46-ΔIII, were generated by high-fidelity PCR using the pTRE-
236 *TGOLN2* plasmid as a template. Each deletion targeted specific domains of the protein as
237 described in Illustration 1, and the oligonucleotides used for amplification are listed in Table 3.
238 To facilitate detection and localization studies, EGFP or FLAG (DYKDDDDK) tags were fused
239 either to the N- or C-terminus of TGN46. Importantly, N-terminal tags were inserted
240 immediately downstream of the signal peptide sequence to preserve the protein's tethering to
241 the secretory pathway. The tagged and truncated TGN46 variants were subcloned into the
242 pLIX402 lentiviral vector (Addgene #41394) using standard molecular cloning techniques
243 detailed in Illustration 1. Lentiviral particles were produced using these constructs, and
244 PDAC087T- *TGOLN2*-KO cells were transduced accordingly. After puromycin selection, cells
245 expressing the tagged or truncated TGN46 variants were used in rescue experiments.

246 **Protein extraction and Western Blot analysis**. For protein extraction, cultured cells grown
247 in 100 mm dishes were washed with ice-cold PBS after removal of the culture medium. PBS
248 was then aspirated, and cells were lysed directly on ice for 10 minutes with 200 µL of RIPA
249 Buffer II, pH 8.0 (Bio Basic – RB4476) supplemented with protease inhibitor cocktail (Sigma-
250 Aldrich – P8340). Lysates were scraped on ice and collected in 1.5 mL microcentrifuge tubes.
251 Cell lysates were sonicated (e.g., 3 cycles of 5 seconds ON / 10 seconds OFF at 30%
252 amplitude using a probe sonicator; adjust based on equipment), followed by centrifugation at
253 13,000 × g for 10 minutes at 4 °C. The clarified supernatants were transferred to fresh tubes,
254 and protein concentrations were determined using the Bradford reagent (SERVA – 39222.03).
255 A fixed amount of protein (30 to 80 µg per sample) was denatured in Laemmli buffer by heating
256 at 95 °C for 5 minutes, then immediately loaded on 10–12% SDS-polyacrylamide gels (Sigma-
257 Aldrich – A3699). Electrophoresis was performed using TG-SDS running buffer (Euromedex –
258 EU0510). Proteins were transferred to nitrocellulose membranes using the Trans-Blot®
259 Turbo™ RTA Transfer Kit and Transfer System (Bio-Rad – 1704271 and 1704150EDU).
260 Transfer efficiency was verified by Ponceau S staining. Membranes were blocked for 30
261 minutes at room temperature (RT) on a rocking platform in TBS-T (TBS with 0.1% Tween-20;
262 Sigma-Aldrich – P1379) containing 5% non-fat dry milk (Millipore – 70166). After blocking,
263 membranes were incubated overnight at 4 °C with primary antibodies diluted in TBS-T + 1%
264 milk, according to the manufacturers' recommendations. The next day, membranes were
265 washed three times for 10 minutes at RT in TBS-T, then incubated for 1 hour at RT with
266 secondary HRP-conjugated antibodies diluted in TBS-T + 1% milk. After washing again (3×10
267 min, RT), detection was performed using the Clarity Western ECL substrate (Bio-Rad – 170-
268 5061), and signal acquisition was carried out with the ChemiDoc™ XRS+ System and Image
269 Lab™ Software (Bio-Rad – 1708265). All antibodies used, along with their sources and working
270 dilutions, are listed in Table 4. Rabbit antisera against H-1PV NS1 and VP were generously
271 provided by Dr. Jürg Nüesch (DKFZ, Heidelberg, Germany)[26].

272 **Viability assays**. Cells were seeded in white-bottom 96-well plates (Greiner Bio-One –
273 675075) at a density of 1×10^4 cells per well in 100 µL of complete medium, in the presence or
274 absence of dox. The following day, cells were incubated for 1 hour at 37 °C with 25 µL of
275 infection medium containing or not H-1PV, applied across 10 different MOIs using a 1:2 serial
276 dilution series starting from MOI 100 down to MOI 0.19. Following incubation, wells were
277 washed once with PBS, and 100 µL of fresh complete medium (± dox) was added. At 48 hours
278 post-infection, 100 µL of CellTiter-Glo® Luminescent Cell Viability reagent (Promega – G7572)
279 was added per well. Plates were mixed for 2 minutes on an orbital shaker to ensure complete
280 cell lysis and reagent mixing. Luminescence was measured as Relative Luminescence Units
281 (RLU) using a TriStar² LB 942 plate reader (Berthold Technologies). For normalization, non-

282 infected control wells were used to define 100% viability, and values from infected conditions
283 were expressed as percentages relative to this reference.

284 **Cell counting**. Cells were seeded in 24-well plates at a density of 4.5×10^4 cells per well in
285 0.5 mL of complete DMEM, with or without dox. For each condition, four replicate wells were
286 prepared, and a separate plate was used for each time point (4 h, 24 h, 48 h, and 72 h). The
287 following day, cells were incubated for 1 hour at 37 °C with 250 µL of infection medium (IM), in
288 the presence or absence of H-1PV, at MOIs of 2.5 or 10. After incubation, wells were washed
289 three times with PBS, and 0.5 mL of fresh complete medium (± dox) was added. For cell
290 counting, 200 µL of the cell suspension was diluted in 20 mL of ISOTON II diluent (Beckman
291 Coulter – 8448011) and analyzed using a Coulter Z1 Particle Counter (Beckman Coulter).

292 **Viral genome quantification by RT(q)PCR**. To assess virus production by infected cells, cells
293 were seeded in 24-well plates at a density of 4.5×10^4 cells per well in 0.5 mL of complete
294 DMEM, with or without doxycycline (dox). For each condition, four replicate wells were
295 prepared, and a separate plate was used for each time point (4 h, 24 h, 48 h, and 72 h). The
296 following day, cells were incubated for 1 hour at 37°C with 250 µL of infection medium, in the
297 presence or absence of H-1PV, at MOIs of 2.5 or 10. After incubation, wells were washed three
298 times with PBS, and 0.5 mL of fresh complete medium (± dox) was added. At each indicated
299 time point, supernatants were collected and diluted 1:2 in PBS in individual 1.5 mL tubes for
300 analysis of released virus. To monitor intracellular viral genome accumulation, cells were
301 seeded in 24-well plates at a density of 2×10^5 cells per well in 0.5 mL complete DMEM ± dox,
302 aiming for a full monolayer by the next day. Plates were prepared with four replicate wells per
303 condition, and a dedicated plate was used for each time point (15 min, 1 h, 2 h, and 4 h). Cells
304 were infected with 250 µL of IM ± dox, ± H-1PV at MOIs of 2.5 or 10. At each time point,
305 supernatants were aspirated, cells were washed four times with PBS, and detached with 250
306 µL trypsin for 5 minutes at 37°C. The reaction was stopped by adding 250 µL of complete
307 DMEM, and cells were thoroughly dissociated. Four hundred microliters of each cell
308 suspension were diluted in 600 µL PBS (cell fraction) and transferred into 1.5 mL microtubes.
309 Samples (1 mL total) were freeze-thawed three times using liquid nitrogen, then centrifuged at
310 12,000 × g for 10 minutes at 4°C. Supernatants were collected for qPCR analysis. For
311 quantification of viral genomes, MicroAmp™ Fast Optical 96-Well Reaction Plates (Invitrogen
312 – 4346906) were filled with 18 µL of qPCR mix, composed of 10 µL SsoFast™ EvaGreen®
313 Supermix (Bio-Rad – 1725204), 0.66 µL of each oligonucleotide (10 µM): Forward: 5′-
314 GCGCGGCAGAATTCAAACT-3′ and Reverse: 5′-CCACCTGGTTGAGCCATCA-3′, and 7.88
315 µL DNAse/RNAse-free water. Then, 2 µL of each sample was added to individual wells. A
316 standard curve was generated using serial dilutions of the pSR19 plasmid, kindly provided by
317 Dr. Jean Rommelaere, which contains the full H-1PV genome. Known copy numbers of pSR19

318 were used to calculate genome copy numbers in each sample. Fast RT-qPCR was performed
319 using the StepOnePlus™ Real-Time PCR System (Applied Biosystems – 4376600), and data
320 were analyzed with StepOne Software v2.3.

321 **Immunofluorescence and viral proteins detection**. Cells were seeded in 24-well plates at
322 a density of 4.5×10^4 to 8×10^5 cells per well on 14mm coverslips (Knittel Glass - 100041) with
323 1 mL of complete DMEM, with or without dox, and incubated at 37°C. The following day, cells
324 were incubated for 1 hour at 37°C with 250 µL of infection medium, in the presence or absence
325 of H-1PV at MOIs of 1 or 2.5. After the incubation, the cells were washed three times with PBS
326 and replaced with 1 mL of complete medium (± dox) and incubated for an additional 24 hours
327 at 37°C. At the end of the incubation, cells were washed with PBS and fixed with PBS-PFA 4%
328 (Electron Microscopy Science - 15710) for 15 minutes at room temperature. After fixation, cells
329 were washed three times with PBS, permeabilized with PBS-Triton X-100 0.25% (Sigma-
330 Aldrich - 93443) for 20 minutes at room temperature, washed three times with PBS, and
331 blocked in PBS-BSA 5% (Euromedex - 04-100-812-E) for 30 minutes at room temperature.
332 For the immunodetection of proteins of interest, cells were incubated with primary antibody
333 diluted in 200 µL of PBS-BSA 1% for 2 hours at room temperature with stirring. After primary
334 antibody incubation, cells were washed three times for 5 minutes with PBS and then incubated
335 with secondary antibody diluted in 200 µL of PBS-BSA 1% for 1 hour at room temperature with
336 stirring. Cells were then incubated with PBS containing DAPI at 0.5 µg/mL (Euromedex -
337 1050A) for 10 minutes at room temperature. After DAPI staining, cells were washed three times
338 for 5 minutes with PBS. Finally, cells were mounted on glass slides with 10 µL of fluorescent
339 mounting medium (Dako - 53023). Image acquisition was performed using a widefield
340 microscope (ZEISS - AxioObserver Z1) with a 10X objective or a confocal microscope (ZEISS
341 - LSM880 Fast Airyscan) with a 63X objective. Images were analyzed with ImageJ 1.53o
342 software. DAPI staining was used to determine the number of cells per field, and fluorescence
343 intensity and area were normalized accordingly. All antibodies used, including dilutions, are
344 listed in Tablexxx. Rabbit antisera directed against H-1PV capsid were kindly provided by Dr.
345 Jürg Nüesch (DKFZ, Heidelberg, Germany).

346 **Viral particles co-localization studies and binding kinetics**. For co-localization studies,
347 cells were seeded in 24-well plates at a density of 4.5×10^4 cells per well on 14 mm coverslips,
348 in 1 mL of complete DMEM supplemented with or without dox, and incubated for 48 hours at
349 37 °C. To assess viral entry, cells were pre-incubated for 15 minutes on ice, followed by a 1-
350 hour incubation on ice with 250 µL of infection medium containing H-1PV at a MOI of 250, in
351 the presence or absence of dox. Cells were transferred to 37 °C to allow synchronized viral
352 entry. For binding kinetic assays, cells were first incubated for 2 hours at 37 °C with 0.5 mL of
353 complete DMEM, with or without dox, and with or without hydroxy-dynasore, a dynamin

354 inhibitor. Cells were then incubated with 250 µL of IM supplemented with the same conditions
355 (± dox, ± hydroxy-dynasore) and H-1PV at a MOI of 250, and maintained at 37 °C. At various
356 time points ranging from 0 minutes to 4 hours post-infection, cells were extensively washed
357 with PBS to remove unbound virus and immediately processed for immunofluorescence
358 staining, as described previously.

359 **GFP-Trap**. On day 0, cells were seeded in 100 mm dishes at a density of 1.5×10^6 cells per
360 dish in 10 mL of complete DMEM supplemented with doxycycline. On day 1, H-1PV was added
361 directly to the culture medium at a MOI of 2.5. On day 4, protein extraction was performed as
362 previously described. GFP-Trap was then carried out using agarose beads coupled with highly
363 specific anti-GFP nanobodies (Proteintech – gta), following the manufacturer's instructions.
364 Briefly, cell lysates were diluted with 300 µL of dilution buffer (10 mM Tris-HCl, 150 mM NaCl,
365 0.5 mM EDTA, pH 7.5) supplemented with 25 µL of GFP-Trap beads, and incubated for 1 hour
366 at 4 °C on a rotating wheel. Beads were collected by centrifugation at 2,500 × g for 2 minutes
367 at 4 °C and washed four times with wash buffer (dilution buffer supplemented with 0.05% NP-
368 40) to remove unbound proteins. Finally, bead-bound proteins were eluted by heating for
369 5 minutes at 95 °C in 2X Laemmli buffer. For Western blot analysis, 50 µL of input lysate (I),
370 flow-through (FT, unbound proteins), and bead-bound fraction (B) were loaded per sample.

371 **Statistics and Reproducibility.** No sample size calculation was performed. All experiments
372 were conducted with at least three biologically independent replicates, and each experiment
373 included a minimum of three technical replicates. No data were excluded from the analysis.
374 Calculations were performed using Microsoft Excel Professional Plus 2016. Statistical
375 analyses were carried out using GraphPad Prism version 10.1.2. For comparisons involving
376 two or fewer groups, unpaired two-tailed Student's t-tests were used. For comparisons
377 involving more than two groups, ordinary one-way ANOVA was performed. In both cases, a
378 95% confidence interval was applied. In micrographs, p-values are indicated as follows: ns for
379 non-significant ($p > 0.05$), * for $p \leq 0.05$, ** for $p \leq 0.01$, *** for $p \leq 0.001$, and **** for $p \leq 0.0001$.
380 Unless otherwise specified, error bars on micrographs represent standard deviation (S.D.).

381 **Data availability**. All data generated or analyzed during this study are included in this
382 published article and its supplementary information files. Access to raw data will be made
383 available upon reasonable request to the corresponding author.

384 **Competing interests**. CM is employee of F. Hoffmann-La Roche. The other authors declare
385 no competing interests.

386

387 **Results**

388 **CRISPR/Cas9 KO screen identifies host genes for H-1PV infection in PDAC cells**. To
389 uncover host factors essential for H-1PV infection, we performed a genome-wide CRISPR-
390 Cas9 knockout screen using the lentiviral GeckoV2 sgRNA library in the PDAC087T primary
391 pancreatic cancer primary culture (Fig. 1A). This model was selected for its biological
392 relevance, robust proliferation, amenability to lentiviral transduction, and susceptibility to H-
393 1PV-mediated oncolysis. Following Cas9 expression and library transduction, cells were either
394 mock-treated or infected with H-1PV. Genomic DNA was extracted one week post-infection,
395 and integrated sgRNA sequences were PCR-amplified and subjected to next-generation
396 sequencing. MAGeCK analysis identified 19 candidate genes whose loss conferred resistance
397 to H-1PV infection (Fig. 1B). To validate these candidates, we conducted a secondary screen
398 in which each gene was targeted using two independent sgRNAs expressed transiently. Three
399 non-targeting sgRNAs served as negative controls. Transfected cells were challenged with H-
400 1PV, and cell viability was quantified 48 hours later (Fig. 1C-D). Knockout of *GAD2*, *MSLN*,
401 *CORO7*, and *ACTL7B* did not significantly alter sensitivity to H-1PV, suggesting these
402 represent false positives or context-dependent hits. In contrast, loss of *SLC35A1*, *SLC35A2*,
403 *CMAS*, *ST3GAL4*, *TGOLN2*, *UNC50*, *GOSR1*, *VPS51*, *VPS54*, *PTAR1*, *COG1*, *COG3*, *COG4*,
404 or *SEC61B* led to reproducible protection from virus-induced cytotoxicity in at least one sgRNA
405 per gene, supporting their functional involvement in H-1PV infection.

406 To gain insight into the functional landscape of candidate H-1PV host factors, we conducted
407 gene ontology enrichment analysis using the PANTHER classification system (Table 5). This
408 analysis highlighted several significantly enriched biological processes, including nucleotide
409 sugar transport, retrograde trafficking at the trans-Golgi network (TGN), intra-Golgi vesicular
410 transport, sialic acid metabolism, and coatomer protein complex I (COPI)-mediated
411 anterograde transport from the endoplasmic reticulum (ER) to the Golgi apparatus. Notably,
412 many identified genes are involved in vesicle-mediated trafficking, suggesting a model in which
413 H-1PV co-opts host transport machinery for efficient intracellular trafficking and infection.
414 Among the candidate genes, we focused on *TGOLN2*, which encodes the glycoprotein TGN46,
415 a conserved sialylated glycoprotein predominantly localized to the TGN, where it functions in
416 the sorting of cargo destined for secretion[20]. Furthermore, a fraction of TGN46 also traffics to
417 the plasma membrane, where it interfaces with components of clathrin-mediated endocytosis
418 (CME)[27], a process that was shown to be critical for efficient H-1PV entry[17]. Given the strong
419 protective phenotype observed upon *TGOLN2* knockout (Fig. 1C-D) and its known roles in
420 endocytic and secretory pathways, we hypothesized that TGN46 facilitates a key step in H-
421 1PV entry or intracellular trafficking, warranting further mechanistic investigation.

422 ***TGOLN2* knockout and overexpression models demonstrate a strong dependency of H-**
423 **1PV on TGN46 for successful infection.**

424 To determine whether TGN46 is required for H-1PV infection, we first performed loss-of-
425 function experiments using gene knockout (KO). We generated PDAC087T cells deficient for
426 *TGOLN2* (PDAC087T-KO) using a non-integrative strategy to minimize permanent genetic
427 alterations and reduce off-target effects associated with constitutive Cas9 expression[28] (Fig.
428 S1A). Efficient TGN46 depletion was confirmed at the protein level by western blotting (Fig.
429 S1B) and immunofluorescence (Fig. S1C). PDAC087T-KO cells demonstrated complete
430 protection from infection at MOI 2.5 or 10 (Fig. 2A), whereas control cell numbers decreased
431 by 35% ± 9% ($p < 0.004$) and 67% ± 9% ($p < 0.001$), respectively (Fig. 2A). We next extended
432 this analysis to HeLa cervical cancer cells, a model known to be permissive to H-1PV
433 infection[29]. Western blot confirmed the *TGOLN2* KO (Fig. S1D). Viability assays performed 48
434 hours post-infection showed that *TGOLN2* KO resulted in a significant reduction in H-1PV-
435 induced oncolysis compared with their respective control cells (Fig. S1E), indicating that
436 TGN46 may function as a conserved host factor for H-1PV infection. We then measured viral
437 genome content in wt and PDAC087T-KO cells following infection with H-1PV. Consistent with
438 the reduction in oncolysis, viral replication was strongly impaired in the absence of TGN46.
439 Quantification of viral DNA by qPCR revealed a significant decrease in intracellular H-1PV
440 genome copies in *TGOLN2*-deficient cells compared with controls (-94% ± 0.5%, $p < 0.01$ and
441 -82% ± 5.6%, $p < 0.001$ for MOI 2.5 and MOI 10, respectively; Fig. 2B). To assess whether
442 this defect translated into altered production of infectious viral particles, we next quantified
443 extracellular H-1PV virions in culture supernatants. TGN46-deficient PDAC087T cells released
444 significantly fewer viral particles compared with control cells, as measured by qPCR-based
445 particle quantification (-73% ± 31%, $p < 0.001$, and -71% ± 11%, $p < 0.001$, at MOI 2.5 and
446 MOI 10, respectively Fig. 2C). These findings indicate that TGN46 loss impairs intracellular
447 viral genome amplification and limits productive virion generation. We next assessed viral
448 protein expression by immunofluorescence. In control cells, robust expression of NS1 and
449 capsid viral protein was readily detected, with a characteristic intracellular distribution (Fig. 2D-
450 E). In contrast, *TGOLN2*-deficient cells consistently displayed a marked reduction in the
451 proportion of infected cells (-74% ± 18%, $p < 0.001$ for NS1 and -85% ± 11%, $p < 0.001$ for
452 capsid proteins, respectively Fig. S1F-G), consistent with impaired viral gene expression. We
453 then assessed whether TGN46 overexpression was sufficient to modulate viral infection and
454 efficacy. To this end, we established PDAC087T cells in which TGN46 overexpression is
455 induced upon doxycycline (dox) treatment (Fig. S1H). Western blotting (Fig. S1I) and
456 immunofluorescence (Fig. S1J) for TGN46 validated both cellular models. We next assessed
457 the impact of TGN46 overexpression following infection with H-1PV at various MOI.

458 Proliferation assays indicated that doxycycline treatment did not affect cell growth, and
459 revealed that TGN46 overexpression resulted in 25% ± 4% ($p < 0.004$) and 31% ± 4% ($p <$
460 0.03) reduced viability at MOI 2.5 and 10, respectively (Fig. 2F). Furthermore, intracellular viral
461 genome content was significantly higher in cells overexpressing TGN46, compared with control
462 cells, with a 2.4 ± 0.2-fold ($p < 0.01$) and 1.5 ± 0.3-fold ($p < 0.002$) increase at MOI 2.5 and 10,
463 respectively (Fig. 2G). In contrast, viral genome levels detected in the culture supernatant,
464 reflecting released progeny virions, were not significantly altered (Fig. 2H). Together, these
465 findings are consistent with a role for TGN46 in early stages of the H-1PV infectious cycle
466 rather than in late steps of virion production or release. Finally, Immunofluorescence analysis
467 further showed enhanced viral protein expression upon TGN46 overexpression. Twenty-four
468 hours post-infection at MOI 2.5, TGN46-overexpressing cells exhibited a significant increase
469 in the percentage of NS1 (1.7-fold ± 0.5, $p<0.05$, Fig. 2I and Fig. S1K) and conformed viral
470 capsid-positive cells (3.6-fold ± 0.9, $p<0.01$, Fig. 2J and Fig. S1L) compared with controls,
471 consistent with increased viral gene expression and productive infection. Taken together,
472 these complementary loss- and gain-of-function experiments identify *TGOLN2*/TGN46 as a
473 host factor that promotes productive H-1PV infection, consistent with a role at an early stage
474 of the viral life cycle, potentially at or upstream of viral entry.

475 **TGN46 regulates H-1PV entry and co-localizes with H-1PV virions at the cell membrane.**
476 Given TGN46's involvement in protein secretion and vesicular recycling, we sought to
477 determine whether its role in H-1PV infection might be indirect, affecting endocytosis
478 pathways, or if TGN46 directly contributes to the virus's attachment or entry into cells. To
479 investigate this, we performed immunofluorescence analyses to assess the steady-state levels
480 of major endocytosis markers of CME in both PDAC087T-KO and PDAC087T cells
481 overexpressing TGN46. Confocal microscopy images were analysed to quantify expression
482 levels, vesicle numbers, and average vesicle sizes using Clathrin Heavy Chain (CHC), Rab5a
483 (early endosome marker), EEA1 (early-intermediate endosome marker), and LAMP1
484 (lysosomal marker). Single-cell quantification revealed that *TGOLN2* knockout or
485 overexpression did not generally alter the expression levels of these endocytic markers, with
486 the exception of EEA1, whose relative signal was increased in *TGOLN2*-depleted cells (Fig.
487 S2A-B). *TGOLN2* downregulation also induced significant changes in both the number (CHC,
488 Rab5a, EEA1) and size (CHC, Rab5a, EEA1) of endocytic vesicles, whereas TGN46
489 overexpression had no detectable effect. To assess whether these morphological alterations
490 affected CME functionality, we performed transferrin uptake assays using Alexa-647-
491 conjugated transferrin (TFn-647), which is internalized exclusively via CME[30]. After a 5-minute
492 incubation, no differences in total TFn-647 uptake were observed between *TGOLN2* knockout,
493 TGN46-overexpressing, and wild-type cells (Fig. S2A-B). However, the number of transferrin-

494 positive vesicles was reduced in *TGOLN2*-depleted cells. Together, these data indicate that
495 modulation of TGN46 expression does not impair the overall capacity for CME in PDAC087T
496 cells.

497 Based on these observations, we next investigated whether TGN46 plays a specific role during
498 the early stages of H-1PV entry. To address this, we performed an H-1PV internalization assay.
499 PDAC087T cells were incubated with H-1PV, and at the indicated time points, cells were
500 washed to remove unbound virus (Fig. 3A). Viral genome content was then quantified by
501 qPCR. At 2 hours post-infection, *TGOLN2*-KO cells contained 45% fewer viral genomes than
502 wild-type controls (Fig. 3A, $p<0.005$), whereas TGN46-overexpressing cells exhibited more
503 than a twofold increase in viral genome levels as early as 15 minutes post-infection (Fig. 3B).
504 These results indicate that TGN46 enhances early H-1PV entry in a dose-dependent manner.
505 To further investigate the role of TGN46 during H-1PV entry, we adapted a previously
506 described synchronization protocol[17] to visualize the interaction between TGN46 and H-1PV
507 using an antibody recognizing conformational capsid epitopes in intact virions. Vesicular
508 trafficking was transiently inhibited in PDAC087T cells by incubation at 4°C for 15 minutes,
509 followed by exposure to a high viral input (MOI 250) for 1 hour at 4°C to allow virus binding
510 without internalization. Viral entry was subsequently initiated by shifting cells to 37°C, and cells
511 were fixed at 5 and 20 minutes post-release. TGN46 and H-1PV capsid were detected by
512 immunostaining, and samples were imaged using super-resolution confocal microscopy. In
513 PDAC087T cells overexpressing TGN46, a pronounced accumulation of H-1PV capsid was
514 observed at the cell periphery as early as 5 minutes post-release (Fig. 3C, left panel). At 20
515 minutes post-release, extensive viral internalization was detected in TGN46-overexpressing
516 cells, with significant co-localization of the viral capsid within TGN46-positive vesicles,
517 consistent with trafficking through TGN-associated compartments (Fig. 3C, right panel).
518 Comparable capsid-TGN46 co-localization was also observed in wild-type PDAC087T cells,
519 although it occurred at later time points (60 minutes post-release) and with reduced TGN46
520 accumulation (Fig. S2C). Notably, cells in prophase, a stage characterized by fragmentation
521 of the TGN and disruption of vesicular trafficking, displayed an accumulation of TGN46/capsid-
522 positive vesicles (Fig. S2D), consistent with a block at an early stage of viral entry.

523 To determine whether TGN46 interacts with the H-1PV virions at the cell surface prior to
524 internalization, as would be expected for a functional viral receptor, we explored experimental
525 conditions that stabilize TGN46 at the plasma membrane. Owing to its rapid recycling kinetics,
526 visualization of surface-localized TGN46 under steady-state conditions is technically
527 challenging. Previous studies have shown that inhibition of dynamin I impairs the scission of
528 clathrin-coated pits, resulting in the accumulation of TGN46 at the cell surface and a
529 concomitant block in CME[31]. We therefore treated PDAC087T cells with increasing

530 concentrations of hydroxy-dynasore, a reversible, non-competitive inhibitor of dynamin I, to
531 phenocopy this condition. To validate CME inhibition, we monitored uptake of transferrin-
532 Alexa647 (TFn-647) after 5 minutes of incubation and quantified fluorescent intensity and area
533 by immunofluorescence (Fig. S2E-F). As expected, TFn-647 internalization was dose-
534 dependently inhibited by dynasore, with near-complete blockade at 100 μM (-95% ± 1.5%,
535 $p<0.001$, Fig. S2F). In parallel, total TGN46 levels remained unchanged (Fig. S2E and S2G),
536 whereas the spatial distribution of the protein shifted, with a significant increase in membrane-
537 associated signal, consistent with plasma membrane accumulation (3.1-fold ± 0.2, $p<0.001$,
538 Fig. S2E and S2H). We next assessed whether surface-localized TGN46 engages the H-1PV
539 capsid. PDAC087T-*TGOLN2*-KO cells reconstituted with a doxycycline-inducible *TGOLN2*-
540 GFP construct were used to compare TGN46-high and TGN46-low cells. Cells were pretreated
541 with dynasore or DMSO and exposed to H-1PV under synchronized infection conditions. At
542 defined time points, cells were immunoassayed for H-1PV capsid proteins and either Rab5a
543 (Fig. 3D) or EEA1 (Fig. 3E) to label early endosomes; TGN46-GFP was detected directly via
544 GFP fluorescence. Under control conditions, TGN46-high cells showed greater accumulation
545 of H-1PV capsids compared to TGN46-low cells, with both TGN46 and capsid signals
546 progressively localizing to Rab5a+ and EEA1+ endosomes. In contrast, dynasore treatment
547 prevented internalization, resulting in co-localization of TGN46 and capsids at the plasma
548 membrane, without detectable overlap with Rab5a or EEA1 (Fig. S2I). These results indicate
549 that TGN46 engages H-1PV at the cell surface within Rab5a-enriched microdomains prior to
550 CME. Collectively, our data identify TGN46 as a novel entry factor for H-1PV that transiently
551 localizes to the plasma membrane to mediate viral engagement before internalization.

552 **TGN46 domain I interacts with H-1PV capsid proteins for successful infection**. To
553 elucidate the mechanism underlying the interaction between TGN46 and H-1PV, we used
554 AlphaFold 2.0 to predict potential structural interfaces between the lumenal domain of TGN46
555 and the viral capsid proteins. We submitted the full lumenal sequence of TGN46, which
556 behaves as an intrinsically disordered region (IDR) and is therefore challenging to model,
557 together with the full VP2 sequence, to AlphaFold (Fig. 4A). This analysis generated five
558 models, which were evaluated using the predicted local distance difference test (pLDDT),
559 predicted aligned error (PAE), predicted template modeling score (pTM), and interface pTM
560 (ipTM) (Fig. 4B). As expected, the high flexibility of the IDR resulted in low ipTM values;
561 however, the top-ranked model showed moderate confidence (pLDDT = 62.7, pTM = 0.618,
562 ipTM = 0.212). Notably, all five models converged on a predicted interaction between domain
563 I of TGN46 and the sialic acid (SIA)-binding pocket of VP2 (Fig. 4B). To improve modelling
564 accuracy, we truncated the input sequences to include only the first 50 amino acids of TGN46
565 domain I and the SIA-binding pocket of VP2. This refinement resulted in a marked increase in

566 prediction scores (pLDDT = 87.6, pTM = 0.855, ipTM = 0.372), supporting a higher-confidence
567 interaction model between TGN46 domain I and VP2.

568 To functionally validate these predictions, we conducted TGN46 rescue experiments in
569 PDAC087T *TGOLN2* KO cells. Cells were transduced with lentiviral vectors encoding dox-
570 inducible *TGOLN2* fused to a FLAG tag at either the N- or C-terminus (Fig. S3A). Control
571 conditions included empty vectors or EGFP alone. Truncated versions of TGN46 lacking
572 individual lumenal domains (ΔI, ΔII, ΔIII) were also generated, with the signal peptide
573 preserved. Immunofluorescence confirmed proper expression of all constructs (Fig. S3B). We
574 then assessed the ability of FLAG-tagged TGN46 variants to rescue H-1PV infection in
575 PDAC087T-KO cells. Following H-1PV infection, infectivity was measured by
576 immunofluorescence detection of conformational capsid proteins. C-terminally FLAG-tagged
577 TGN46 fully restored H-1PV infectivity in PDAC087T-KO cells (Fig. 4C). We also generated a
578 C-terminally GFP-tagged version of TGN46, which was validated for proper expression (Fig.
579 S3C) and similarly rescued infection in PDAC087T-KO cells (Fig. S3D). In contrast, N-
580 terminally tagged constructs failed to restore infectivity (Fig. 4C, Fig. S34). Among the domain-
581 deletion mutants, the ΔII and ΔIII variants supported infection at levels comparable to full-
582 length TGN46, whereas the ΔI mutant failed to restore infectivity, indicating that luminal domain
583 I (32 amino acids) is essential for H-1PV infection (Fig. 4C).

584 To assess whether TGN46 physically associates with the H-1PV capsid, we performed GFP-
585 TRAP co-immunoprecipitation assays in PDAC087T-WT cells transduced with EGFP-tagged
586 TGN46 constructs. Following H-1PV infection, GFP fusion proteins were immunoprecipitated
587 using anti-GFP nanobodies (Fig. S3E). Western blot analysis revealed that the viral capsid
588 proteins VP1 and VP2 co-immunoprecipitated specifically with C-terminally tagged TGN46
589 variants, indicating that TGN46 and the H-1PV capsid belong to the same molecular complex
590 (Fig. 4D). Notably, under these conditions, TGN46 did not associate with the viral protein NS1
591 nor with galectin-1 (Fig. S3H). Domain-deletion analysis showed that TGN46 variants lacking
592 domains II or III retained capsid interaction, whereas deletion of domain I (ΔI) reduced VP1
593 and VP2 binding by 75% and 65%, respectively (Fig. 4D). Considering the critical role of protein
594 glycosylation in H-1PV infection[14], we investigated the contribution of post-translational
595 modifications in TGN46 and H-1PV interaction. TGN46-EGFP expressing cells were treated
596 with neuraminidase (NA), that cleaves sialic acid residues from glycoproteins and glycolipids
597 on the cell surface. We found that NA treatment significantly inhibited H-1PV entry (- 53% ± 15
598 %, $p<0.05$, Fig. S3I) and induced a mobility shift of mature TGN46 (Fig. 4D). Importantly, NA
599 treatment decreased co-immunoprecipitation of VP1 and VP2 by 50% and 35%, respectively
600 (Fig. 4D). To further probe the role of glycosylation in TGN46-mediated H-1PV entry, we
601 mutated the sole predicted N-glycosylation site within domain I by at asparagine 39 (N39) to

602 glutamine (Q), a conservative substitution that prevents glycosylation while preserving local
603 structure. This N39Q mutation reduced VP1 binding by 35% without affecting VP2 interaction,
604 indicating that this glycosylation contributes to the VP1-TGN46 association (Fig. 4D). Together,
605 these results demonstrate that TGN46 binds H-1PV capsid proteins through domain I, and
606 confirms that sialylated glycosylation is an important determinant of this interaction.

607 **TGN46 is a key determinant of H-1PV entry and oncolytic activity in PDAC cells**. Given
608 that mechanistic studies have collectively identified TGN46 as a critical mediator of H-1PV
609 entry, we next examined whether this dependency dictates the specificity and the oncolytic
610 efficacy of H-1PV in PDAC cells. H-1PV entry was quantified across a panel of PDAC-derived
611 cell lines following infection with an MOI of 200 of the virus, using normal pancreatic ductal
612 epithelial (HPDE) cells as a non-malignant control. HPDE cells exhibited remarkably low levels
613 of viral entry ($1.3x10^4$ a.u. ± $0.7x10^4$), which were significantly lower than those observed in
614 Capan-2 ($4x10^4$ a.u. ± $2.7x10^4$, $p < 0.05$), BxPC-3 ($9x10^4$ a.u. ± $2.4x10^4$, $p < 0.0001$), Mia
615 PaCa-2 ($1.1x10^5$ a.u. ± $2.3x10^4$, $p < 0.0001$), and Panc-1 cells ($2.2x10^5$ a.u. ± $4.5x10^4$, $p <$
616 0.0001), the latter showing the highest susceptibility to infection ($p<0.0001$, Fig. 5A). In
617 contrast, AsPC-1 cells did not show a significant difference in H-1PV entry compared to HPDE
618 cells ($2.5x10^4$ a.u. ± $0.6x10^4$, $p = 0.4$; Fig. 5A). We then investigated the half-maximal inhibitory
619 concentration (IC_{50}) of H-1PV on the same panel of cells. Normal HPDE exhibited pronounced
620 resistance to H-1PV, with no measurable IC_{50} (Fig. 5B). Among PDAC cells, AsPC-1 (IC_{50} MOI
621 = 193.2 ± 2.3) and Capan-2 (IC_{50} MOI = 132.6 ±2.1) were classified as resistant, while BxPC-
622 3 (IC_{50} MOI = 19.6 ±1.3), Mia PaCa-2 (IC_{50} MOI = 5.4 ±0.7), and Panc-1 (IC_{50} MOI = 2.8 ±0.45)
623 displayed marked susceptibility to viral cytotoxicity. These same cell lines were subsequently
624 analysed for the protein expression of TGN46, along with two known modulators of H-1PV
625 entry, galectin-1[15,32] and laminin subunit gamma-1 (LAMC1)[33], to explore potential correlations
626 with viral sensitivity. Interestingly, both galectin-1 and LAMC1 were detected in HPDE cells
627 despite their resistance to infection (Fig. S4A). While galectin-1 expression alone showed a
628 positive correlation with H-1PV sensitivity across the panel, LAMC1 levels did not reflect IC_{50}
629 values (Fig. S4A). Remarkably, TGN46 expression was absent in HPDE cells and positively
630 correlated with H-1PV sensitivity in PDAC-derived cells (Fig. S4A).

631 To further investigate the contribution of TGN46 to H-1PV infectivity, we deleted *TGOLN2* in
632 highly susceptible, TGN46-positive Panc-1 cells using CRISPR/Cas9. Loss of TGN46
633 expression was confirmed by Western blot (Fig. S4B) and resulted in a 7.5-fold increase in the
634 H-1PV IC_{50} ($p < 0.0001$; Fig. 5C), indicating reduced viral sensitivity. In mirror studies, we
635 conditionally overexpressed TGN46 in TGN46-low, H-1PV resistant AsPC-1 cells. Dox addition
636 successfully induced TGN46 expression (Fig. S4C, $p<0.0001$), and resulted in an a 6.2-fold
637 induction of H-1PV entry (Fig. 5D, $p<0.0001$) and significant sensitization to H-1PV infection

638 (+35% ± 8, p<0.01, Fig. 5E). We extended our analysis to primary PDAC-derived cultures, as
639 these may better capture tumour heterogeneity than established cell lines and enhance clinical
640 relevance. We quantified H-1PV entry and found that PDAC087T cells exhibited high levels of
641 viral entry (9.7×10^4 a.u. ± 1.3×10^4, $p < 0.0001$; Fig. 5F). Interestingly, these cells expressed
642 the highest protein levels of TGN46 and galectin-1 (Fig. S4D). We then measured the IC_{50} of
643 H-1PV on primary PDAC cells. IC_{50} was not reached for PDAC084T, PDAC072T and
644 PDAC051T cultures, that were classified as resistant, while PDAC091T (IC_{50} MOI = 27.7 ±1.3),
645 PDAC087T (IC_{50} MOI = 8.9 ±0.7), and PDAC012T (IC_{50} MOI = 3.7 ±0.45) were highly
646 susceptible to H-1PV-induced cytotoxic effects. We then applied the same strategy used in
647 established cell lines to assess the role of TGN46 in H-1PV infection of primary cells by deleting
648 *TGOLN2* using CRISPR–Cas9 in susceptible PDAC087T cells. Targeting TGN46 expression
649 resulted in a 19-fold increase in the H-1PV IC_{50} (p<0.0001, Fig. 5H), corresponding to reduced
650 sensitivity to viral infection. Importantly, these results extend our findings from cell lines to
651 primary PDAC cultures and demonstrate that TGN46 contributes not only to H-1PV infection
652 but also to its oncolytic activity. Together, these data warrant further exploration of TGN46
653 function in experimental models *in vivo*.

654 **TGN46 is required for H-1PV antitumoral activity *in vivo***

655 To assess the contribution of TGN46 to H-1PV oncolytic activity *in vivo*, we generated
656 subcutaneous tumors from primary PDAC087T cells in which *TGOLN2* was deleted using
657 CRISPR-Cas9 (Fig. 6A). Efficient and sustained depletion of *TGOLN2* in tumour tissues was
658 confirmed at the protein level by Western blot analysis (Fig.6B). Following two intratumoral
659 administrations of H-1PV, control tumours exhibited a marked reduction in tumour volume
660 ($321.5mm^3 \pm 15.9$ vs $160mm^3 \pm 27.9$, p<0.01) and weight (0.3g±0.04 vs 0.18g±0.02, p<0.05),
661 consistent with robust oncolytic activity, compared to control mice receiving PBS (Fig. 6C and
662 6D). In contrast, *TGOLN2*-deficient tumours failed to respond to H-1PV treatment, showing no
663 significant reduction in tumour volume or mass (Fig. 6E and 6F). Consistent with this loss of
664 therapeutic efficacy, quantification of viral genomes at the experimental endpoint revealed a
665 significant decrease in H-1PV copy number in *TGOLN2*-depleted tumors compared with
666 controls ($4.1x10^3$a.u.$\pm 1.7x10^3$ vs $0.3x10^3$a.u.$\pm 0.1x10^3$, p<0.05, Fig. 6G). Collectively, these
667 results demonstrate that TGN46 expression is required for productive H-1PV infection and
668 oncolytic activity in experimental PDAC tumour models.

669

670 **Discussion**

671 Oncolytic viruses offer a promising approach to selectively target malignant cells while sparing
672 normal tissues[4]. Among these, H-1PV stands out due to its non-pathogenicity in humans, its
673 natural oncotropism and safety in clinical trials[8,9,10]. However, the molecular basis of this
674 selectivity has remained partly defined. Contrary to many OV, the oncoselectivity of
675 parvoviruses in human cells does not appear to rely on impaired innate immunity within cancer
676 cells. Studies have demonstrated that IFN signalling fails to reduce H-1PV infectivity or
677 progeny production in both normal and transformed cells[34,35], despite the upregulation of
678 interferon-stimulated genes (ISGs)[35]. This unexpected resistance to IFN-mediated antiviral
679 responses may stem from either the absence of functional pattern recognition receptor (PRR)
680 expression or intrinsic defects, potentially virus-driven, in the endosomal sensing of parvoviral
681 genomes[36]. Notably, H-1PV susceptibility does not correlate with absolute ISG levels but rather
682 with the efficiency of viral entry. This is exemplified by the cooperative role of laminin γ1[33] and
683 galectin-1[15], the later recently confirmed as a key mediator of H-1PV efficacy during a
684 biomarker screen in PDAC cell cultures[32].Yet, despite that H-1PV efficacy in PDAC appears to
685 rely almost entirely on effective cell entry, the identity of high-affinity cell surface receptors
686 facilitating H-1PV uptake has remained elusive, and definitive biomarkers predicting viral
687 susceptibility remains to be fully established.

688 In this study, we demonstrate that TGN46 is involved early stages of viral entry, supports
689 productive infection, and is required for downstream oncolytic activity. TGN46 is encoded by
690 *TGOLN2* and is widely expressed across various human tissues, particularly in epithelial and
691 secretory cells, where it plays a role in protein sorting and trafficking within the TGN. It functions
692 as a cargo receptor, facilitating the sorting of secretory proteins into specific vesicles for
693 delivery to their destinations[37]. There is no direct link between TGN46 and cancer, but it has
694 been implicated in the formation of CARTS (carriers of the TGN to the cell surface), a PKD-
695 dependent pathway critical for the secretion of specific cargo[38], particularly that of pancreatic
696 adenocarcinoma upregulated factor (PAUF)[39], that is associated with TGFβ-dependent
697 increase in the migration and invasion of PDAC cell lines[40], and possibly in the establishment
698 of an immunosuppressive tumor microenvironment[41].

699 Using for the first time in the filed a combination of genetic perturbation, high-resolution
700 imaging, co-immunoprecipitation, and functional virological assays, we demonstrate that
701 TGN46 transiently localizes to the plasma membrane where it engages the H-1PV capsids in
702 Rab5a-enriched domains, prior to CME. This previously underestimated surface function of
703 TGN46 contrasts with the aforementioned classical role as a resident of the TGN, revealing
704 new insights into the dynamic trafficking of this protein and its potential repurposing in the
705 context of viral entry. This echo recent findings indicating that TGN46 plays a role in the

706 intracellular trafficking of SARS-CoV-2 proteins, especially SARS-CoV-2 E protein that
707 undergoes retrograde trafficking to the TGN, accumulating in LAMP1-positive vesicles, likely
708 lysosomes[42].

709 Our findings position TGN46 as a *bona fide* host factor for H-1PV infection in PDAC cells and
710 TGN46 and H-1PV virions colocalize at the cell membrane. Mechanistically, TGN46 domain I
711 emerges as both necessary and sufficient for H-1PV internalization following interaction with
712 H-1PV capsid proteins, whereas domains II and III were dispensable. Treatment with
713 sialylation inhibitor neuraminidase or mutation of the single predicted glycosylation site within
714 domain I (N39) impaired binding to VP1 but not VP2, suggesting distinct roles for glycan-
715 mediated interactions in capsid recognition. Interestingly, TGN46 does not bind with the non-
716 structural NS1 protein or galectin-1 itself, suggesting that TGN46 may act as a primary
717 attachment or internalization factor rather than a broader viral scaffold. Despite the strength of
718 these findings, our study has several limitations. First, while we have established a physical
719 association between TGN46 and the H-1PV capsid, the precise molecular interface remains
720 undefined. Structural studies, such as cryo-EM or crosslinking-mass spectrometry, could help
721 map the interaction site and guide rational design of virus mutants with improved binding
722 properties. Second, although TGN46 appears to be expressed and localized to the plasma
723 membrane in PDAC cells, the underlying regulation of expression or trafficking mechanisms
724 are unknown. Future work should determine whether this pattern of expression and localization
725 is driven by oncogenic signalling pathways or specific post-translational modifications, and
726 whether it is unique to PDAC or observed in other H-1PV-sensitive tumors.

727 Furthermore, our study uncovers several key insights with significant translational potential.
728 First, we quantified H-1PV infection efficiency across a panel of established PDAC cell lines
729 and primary patient-derived tumor cells. Susceptibility varied markedly, with some cell lines
730 showing robust infection and others remaining refractory. Second, we show that TGN46
731 expression correlates with susceptibility to H-1PV across both cell lines and patient-derived
732 samples. Third, functional studies demonstrate that inducible overexpression of TGN46 in
733 otherwise resistant cells restored susceptibility to infection. In contrast, CRISPR-mediated
734 deletion of *TGOLN2* strongly attenuated viral infectivity and efficacy, both *in vitro* and *in vivo*
735 in experimental tumor models. These data not only validate TGN46 as a host factor for H-1PV,
736 but also indicate that its expression level is rate-limiting for virotherapy efficacy. Collectively,
737 our findings suggest that TGN46 may serve as predictive biomarker of H-1PV responsiveness
738 in PDAC, a notoriously heterogeneous and treatment-refractory malignancy. The ability to
739 stratify PDAC based on TGN46 expression could offer a biomarker-based approach to
740 personalize oncolytic virus therapies. Pre-treatment screening could help identify patients most
741 likely to benefit from virotherapy. Moreover, our data raise the possibility of pharmacologically

742 enhancing TGN46 expression or surface localization to sensitize otherwise refractory tumors.
743 In conclusion, this study reveals an unexpected role for TGN46 in mediating H-1PV entry and
744 positions this protein as a critical determinant of virotherapy responsiveness in PDAC. These
745 insights pave the way for refined biomarker-driven approaches and underscore the value of
746 probing unconventional host-virus interactions in the development of targeted cancer
747 therapeutics.

748

749

750 **Figure legends**

751

752 **Figure 1: CRISPR/Cas9 KO screen identifies TGOLN2 as a host gene for H-1PV infection.**
753 **A.** CRISPR/Cas9 KO screening strategy of H-1PV host genes. PDAC087T cells constitutively
754 expressing Cas9 nuclease enzyme were transduced with the lentiviral pooled sgRNA library
755 GeckoV2 at 0.3 MOI to obtain one gene KO per cell. Cells were then infected with H-1PV or
756 not (NI) at a MOI of 10 and sgRNA content of each population was determined by PCR of
757 sgRNA locus, NGS sequencing and MAGeCK sgRNA enrichment analysis. **B.** Micrograph
758 showing each individual gene screened with an arbitrary gene number in x-axis and the sgRNA
759 positive enrichment score determined with MAGeCK algorithm in y-axis. Genes under positive
760 enrichment score cut-off are drawn with gray dots; genes above cut-off were annotated and
761 grouped by family: sialic acid metabolism (yellow dots), vesicular trafficking / protein secretion
762 (orange dots) and others (teal dots). **C.** Representative validation of gRNA screening results.
763 Examples are shown for control non-targeting gRNAs, for non-validated gRNAs that did not
764 affect viral cytotoxicity (targeting *MSLN*, *CORO7*), and for validated gRNAs that abolished viral
765 lytic activity (targeting *UNC50*, *TGOLN2*). An MOI of 5 was used for H-1PV infection. Cell
766 confluence was monitored using the IncuCyte live-cell imaging system. Data represent the
767 mean ± S.D. of three independent biological experiments performed in triplicate. **D.** Individual
768 validation of genes above positive enrichment score threshold. PDAC087T-Cas9 cells were
769 transduced to express stably individual sgRNAs of each gene to validate (2 sgRNA per gene
770 and 3 non-targeting human control sgRNAs), then cells were infected or not with H-1PV at MOI
771 5. 48h post infection, cell viability assay was performed and survival ratio (infected / NI)
772 calculated for each sgRNA. Mean ratios of the three non-targeting human controls sgRNA
773 were pooled (P, red dots) and use as reference to calculate resistance to H-1PV conferred by
774 each individually tested sgRNA (% variation of infected / NI). Negative value stands for
775 increased sensitivity to infection. Dots and bars colors correspond to target gene family: non-
776 targeting (gray and light gray), sialic acid metabolism (yellow), vesicular trafficking (orange)
777 and others (blue). For statistical analysis, Fisher's LSD multiple comparisons test was
778 performed.

779

780 **Figure 2: H-1PV rely on TGN46 expression for successful infection and oncolytic**
781 **activity.** (**A, F**) cell counts, (**B, G**) intracellular H-1PV viral genomes content (qPCR targeting
782 the NS1 genomic locus) and (**C, H**) H-1PV viral genomes in the supernatant of PDAC087T-
783 WT and *TGOLN2*-KO cells (**A-C**), and control or of TGN46-overexpressing PDAC087T cells
784 (**F-H**), measured 48h post H-1PV infection. Infections were performed at MOI 2.5 and 10.
785 Statistical comparisons were performed using a two-way ANOVA. (D, E) Immunofluorescence

786 (IF) analysis of PDAC087T-WT and *TGOLN2*-KO cells, and (I, J) control or TGN46-
787 overexpressing PDAC087T cells, 24 h post–H-1PV infection at an MOI of 2.5. Cells were
788 stained with anti-TGN46 antibody (green) and DAPI for DNA counterstaining (light gray). Anti-
789 NS1 antibody (orange) and anti-H-1PV conformational capsid antibody (red) were used to
790 detect viral proteins. Images were acquired using a wide-field microscope with a 20X objective
791 (scale bars: 100 µm).

792

793 **Figure 3: Modifications in TGN46 expression level do not impact CME but controls H-**
794 **1PV entry.** PDAC087T-WT (WT) cells, or PDAC087T cells KO for *TGOLN2* (KO-T, **A**), and
795 PDAC087T cells overexpressing (+) or not (-) TGN46 (**B**) were infected with H-1PV at MOI 2.5
796 and incubated 15, 60, 120 or 240 min at 37°C followed with extensive wash with PBS, to
797 remove unbound virus, and internalized viral genomes were quantified by qPCR against NS1
798 genomic locus**.** Statistical comparisons were performed using a two-way ANOVA**. C.** Cells
799 were pre-incubated for 15 min at 4°C and then infected with H-1PV at an MOI of 250 for 1 h at
800 4°C to allow viral binding to the cell surface. Cells were subsequently shifted to 37°C for 5 or
801 20 min, extensively washed with PBS, fixed, and processed for IF staining of TGN46 (green),
802 viral capsid (red), and DAPI for DNA counterstaining (light gray). Images were acquired using
803 a confocal microscope with a 63× objective (scale bars, 20 µm). Regions of interest were
804 magnified 5-fold. PDAC087T-*TGOLN2*-KO cells reconstituted with a doxycycline-inducible
805 TGN46-GFP construct and pretreated for 30 min with DMSO (control, **D** and **E**, left panels) or
806 100µM hydroxy-dynasore (Dyn, **D** and **E**, right panels). Cells were infected with H-1PV at an
807 MOI of 250 for the indicated times, and stained with antibodies against TGN46 and viral
808 capsids (D, E), together with antibodies against Rab5a (**D**) or EEA1 (**E**) and DAPI for DNA
809 counterstaining (light gray)**.** Images were acquired using a confocal microscope with a 63×
810 objective (scale bars, 20 µm).

811

812 **Figure 4: H-1PV infection requires interaction of capsid proteins with sialic acid motifs**
813 **present in TGN46 N-terminal domain I. A**. Predicted model of the interaction between the
814 full luminal domain of TGN46 and H-1PV capsid proteins generated using AlphaFold 2.0. **B**.
815 Model evaluation based on predicted local distance difference test (pLDDT), predicted aligned
816 error (PAE), predicted template modeling score (pTM), and interface predicted template
817 modeling score (ipTM). **C.** PDAC087T-WT cells (gray bars); PDAC087T cells with dox-
818 inducible TGN46 expression (orange bars), PDAC087T-*TGOLN2*-KO cells (green bars); and
819 PDAC087T-*TGOLN2*-KO cells co-expressing dox-inducible FLAG-TGN46, TGN46-FLAG,
820 TGN46ΔI-FLAG, TGN46ΔII-FLAG, or TGN46ΔIII-FLAG (pink bars) were treated with 0, 50, or

821 500 µg/mL dox) and infected with H-1PV at an MOI of 2.5 for 24 h. Cells were fixed and stained
822 with an antibody against H-1PV conformational capsid proteins and DAPI for DNA
823 counterstaining (light gray). Images were acquired using a confocal microscope with a 20×
824 objective. Total capsid fluorescence intensity per cell was quantified and normalized to the
825 control condition (red dotted line). Data represent mean ± SD of three independent
826 experiments performed in triplicate. Statistical analysis was performed using uncorrected
827 Fisher's LSD test**. D.** PDAC087T-*TGOLN2*-KO cells transduced with lentiviral vectors
828 encoding EGFP, EGFP-TGN46, TGN46-EGFP, TGN46ΔI-EGFP, TGN46ΔII-EGFP,
829 TGN46ΔIII-EGFP, or TGN46N39Q-EGFP were infected with H-1PV at an MOI of 2.5. In
830 addition, PDAC087T-*TGOLN2*-KO cells expressing TGN46-EGFP were treated with
831 neuraminidase prior to infection. Two days post-infection, cellular proteins were extracted and
832 incubated with GFP-Trap beads. Bead-bound proteins were resolved by western blot. Input
833 whole-cell lysates and GFP-Trap co-immunoprecipitated proteins were analyzed by western
834 blot for EGFP, VP1, and VP2.

835

836 **Figure 5: TGN46 drives H-1PV entry and oncolytic efficacy in pancreatic ductal**
837 **adenocarcinoma cells. A**. PDAC cell lines were infected with H-1PV (MOI 200) for 2 hours.
838 Cells were then fixed and stained with an antibody targeting the conformational H-1PV capsid
839 protein. Normal pancreatic ductal epithelial (HPDE) cells were used as control. Images were
840 acquired using a confocal microscope (63× objective), and fluorescence intensity was
841 quantified. Data represent the mean ± SD of three independent experiments, each performed
842 in triplicate. Statistical comparisons were performed using a two-way ANOVA. **B**. PDAC cell
843 lines were infected with H-1PV at the indicated MOIs. After 48 hours, cell viability was
844 measured using the CellTiter-Glo (CTG) assay, and IC_{50} values were calculated. Data
845 represent the mean ± SD of three independent experiments, each performed in triplicate. **C**.
846 Panc-1 cells with *TGOLN2* knockout were generated using CRISPR/Cas9 and infected with
847 H-1PV at the indicated MOIs. After 48 hours, cell viability was measured using CTG assay.
848 Data represent the mean ± SD of three independent experiments, each performed in triplicate.
849 Statistical comparisons were performed using an unpaired t-test. Lentiviral vectors encoding
850 for TGN46 were used to generate AsPC-1 TGN46 cells. Proteins expression was induced or
851 not by doxycycline and cells infected with H-1PV at an MOI of 200 for 2 h (**D**). Cells were then
852 fixed and stained with an antibody targeting the conformational H-1PV capsid protein. Images
853 were acquired using a confocal microscope (63× objective), and fluorescence intensity was
854 quantified. Alternatively, AsPC-1 cells expressing or not TGN46 were infected with H-1PV at
855 an MOI of 50. **E.** After 48 hours, cell viability was measured using the CTG assay. Data
856 represent the mean ± SD of three independent experiments, each performed in triplicate.

857 Statistical comparisons were performed using an unpaired t test. **F.** PDAC primary cells were
858 infected with H-1PV (MOI 200) for 2 hours. Cells were then fixed and stained with an antibody
859 targeting the conformational H-1PV capsid protein. Images were acquired using a confocal
860 microscope (63× objective), and fluorescence intensity was quantified. Data represent the
861 mean ± SD of three independent experiments, each performed in triplicate. Statistical
862 comparisons were performed using a two-way ANOVA. **G**. PDAC primary cells were infected
863 with H-1PV at the indicated MOIs. After 48 hours, cell viability was measured using the CTG
864 assay, and IC_{50} values were calculated. Data represent the mean ± SD of three independent
865 experiments, each performed in triplicate. **H**. PDAC087T primary cells with *TGOLN2* knockout
866 were generated using CRISPR/Cas9 and infected with H-1PV at the indicated MOIs. After 48
867 hours, cell viability was measured using CTG assay. Data represent the mean ± SD of three
868 independent experiments, each performed in triplicate. Statistical comparisons were
869 performed using an unpaired t-test.

870

871 **Figure 6: H-1PV antitumoral effects in vivo depend on TGN46. A**. Schematic
872 representation of the in vivo study. PDAC087T-WT or PDAC087T-*TGOLN2*-KO cells were
873 implanted subcutaneously in NSG mice. Eleven days later, experimental tumors received a
874 first intratumoral (IT) injection of 5×10^6 plaque-forming units (p.f.u.) of the virus, followed by
875 a second injection 4 days later. Control mice received two intratumoral injections of PBS.
876 Tumors were sampled and analyzed 7 days after the second viral injection, and TGN46
877 expression was assessed by Western blot (**B**). Tumor volume (**C**, **E**), weight (panels **D**, **F**),
878 were measured, and viral content was quantified by NS1 qPCR (**G**). Data represent the mean
879 ± SD of at least 4-6 animals per group. Statistical comparisons were performed using an
880 unpaired t-test.

881

882 **Figure S1. A.** Schematic representation of the all-in-one plasmid used for CRISPR/Cas9-
883 mediated knockout (KO) of TGN46 (*TGOLN2* sgRNA) by transient transfection followed by
884 ouabain selection. **B.** Western blot analysis of TGN46 expression in PDAC087T-WT and
885 PDAC087T-*TGOLN2*-KO cells. GAPDH was used as loading control. **C.** Immunofluorescence
886 (IF) analysis of PDAC087T-WT (WT) and PDAC087T-*TGOLN2*-KO (KO) cells stained with
887 anti-TGN46 antibody (green) and DAPI for DNA counterstaining (light grey). Images were
888 acquired using a confocal microscope at 63x objective (top row, 20µm scale bars) and regions
889 of interest were magnified 5 times (bottom row). **D.** Western blot analysis of TGN46 expression
890 in Hela cells, and Hela cells expressing *TGOLN2* sgRNA. GAPDH was used as loading control.
891 **E.** Cell viability assay of Hela cells expressing control sgRNA and wild-type for *TGNOL2* (WT),

892 and *TGOLN2*-KO Hela cells (KO) following infection with H-1PV at the indicated MOI. Data
893 represent mean ± S.D. of three independent experiments performed in triplicates. IF analysis
894 of NS1 **(F)** or capsid **(G)** proteins in PDAC087T-WT (WT) and PDAC087T- *TGOLN2*-KO (KO)
895 cells following infection with H-1PV at an MOI of 2.5. Data represent mean ± S.D. of three
896 independent experiments performed in triplicate. Unpaired t-test were performed for statistical
897 analysis. **H.** Schematic representation of all-in-one "pTRE-TGN46" Tet-on lentiviral vector for
898 doxycycline inducible TGN46 overexpression. **I.** Western blot analysis of TGN46 expression
899 in PDAC087T-pTRE-TGN46 cells -/+ dox (TGN46 -/+). HSP90 was used as loading control. **J.**
900 IF of PDAC087T without dox (TGN46 -) and PDAC087T cells overexpressing TGN46 upon
901 dox treatment (TGN46 +), stained with anti-TGN46 antibody (green) and DAPI (light grey).
902 Images were acquired using a confocal microscope at 63X objective (first row, 20µm scale
903 bars) and regions of interest were magnified 5 times. IF analysis of NS1 **(K)** or capsid **(L)**
904 proteins in PDAC087T cells without dox (TGN46 -) and PDAC087T cells overexpressing
905 TGN46 upon dox treatment (TGN46 +), following infection with H-1PV at an MOI of 2.5. Data
906 represent mean ± S.D. of three independent experiments performed in triplicate. Unpaired t-
907 test were performed for statistical analysis.

908

909 **Figure S2. A.** PDAC087T-WT (WT) and PDAC087T-*TGOLN2*-KO (KO) cells, and **(B)**
910 PDAC087T cells without doxycycline (TGN46 −) and PDAC087T cells overexpressing TGN46
911 upon doxycycline treatment (TGN46 +) were stained with antibodies against vesicular
912 transport-related proteins (CHC, Rab5, EEA1, and LAMP1) or analyzed for TFn-647 uptake.
913 Each row shows representative images of staining for one protein of interest (green) or the
914 TFn-647 signal (pink), along with DAPI counterstaining of DNA (light gray). Images were
915 acquired using a confocal microscope with a 63X objective (scale bars: 20 µm). Quantification
916 of total fluorescence intensity, number of objects, and mean object size (µm²) was performed
917 in 30–50 individual cells per condition. Statistical comparisons were conducted using unpaired
918 t tests. PDAC087T-WT cells in interphase **(C)** or prophase **(D)** were stained with antibodies
919 against TGN46 (green) and viral capsids (red), along with DAPI counterstaining of DNA (light
920 gray). Images were acquired using a confocal microscope with a 63× objective (scale bars: 20
921 µm). PDAC087T-WT cells were treated with hydroxy-dynasore (Dyn) at the indicated
922 concentrations and stained with antibodies against TGN46 (green) or analyzed for TFn-647
923 uptake (pink), along with DAPI counterstaining of DNA (light gray). **E.** Images were acquired
924 using a confocal microscope with a 20X objective. Transferrin uptake **(F),** TGN46 fluorescence
925 intensity **(G)** and total TGN46-positive area **(H)** were quantified. Data represent mean ± S.D.
926 of three independent experiments performed in triplicate. Šídák's multiple comparisons test

927 were performed for statistical comparisons. **I.** Representative image and signal quantification
928 showing colocalization of TGN46 (green) and viral capsid (red).

929 **Figure S3. A.** Schematic representation of TGN46 fusion proteins (FLAG or GFP in N-or C-
930 terminal, red box) and deleted variants (domain I, II or III, doted lines) generated for rescue
931 and GFP-TRAP experiments (subcloning in previously described pTRE inducible lentivector).
932 Legends: signal peptide (SP), luminal part (Lum.), cytoplasmic part (Cyto.) and
933 transmembrane domain (IV). **B.** PDAC087T-WT cells, or PDAC087T-*TGOLN2*-KO cells were
934 transduced with empty control lentiviral vectos (pTRE) or lentivial vectors encoding for TGN46,
935 FLAG-TGN46 and FLAG-TGN46 domain I, II or III deleted mutants. Protein expression was
936 induced by doxycycline (dox), and cells were stained with antibodies against FLAG and
937 fluorescence was quantified. Data represent mean of three independent experiments
938 performed in triplicate**.** Statistical comparisons were performed using a two-way ANOVA. **C**.
939 PDAC087T-WT cells, or PDAC087T-*TGOLN2*-KO cells were transduced with empty control
940 lentiviral vectos (pTRE) or lentivial vectors encoding for TGN46, EGFP, EGFP-TGN46 and
941 TGN46-EGFP. Proteins expression was induced by doxycycline (dox), and EGFP
942 fluorescence was quantified. Data represent mean of three independent experiments
943 performed in triplicate**.** Statistical comparisons were performed using a two-way ANOVA. **D**.
944 PDAC087T-WT cells, or PDAC087T-*TGOLN2*-KO cells were transduced with empty control
945 lentiviral vectos (pTRE) or lentivial vectors encoding for TGN46, EGFP, EGFP-TGN46 and
946 TGN46-EGFP. Proteins expression was induced by doxycycline (dox) and infected with H-1PV
947 at an MOI of 2.5 for 24 h. Cells were fixed and stained with an antibody against H-1PV
948 conformational capsid proteins and DAPI for DNA counterstaining (light gray). Images were
949 acquired using a confocal microscope with a 20X objective. Total capsid fluorescence intensity
950 per cell was quantified and normalized to the control condition (red dotted line). Data represent
951 mean ± SD of three independent experiments performed in triplicate. Statistical analysis was
952 performed using uncorrected Fisher's LSD test. **E**. Schematic representation of the GFP-Trap
953 strategy. F. PDAC087T-*TGOLN2*-KO cells transduced with lentiviral vectors encoding EGFP,
954 EGFP-TGN46, or TGN46-EGFP were infected with H-1PV at an MOI of 2.5. Two days post-
955 infection, cellular proteins were extracted and incubated with GFP-Trap beads. Input,
956 flowthrough and bead-bound proteins were resolved by western blot for EGFP, VP1, VP2,
957 NS1, GAPDH, and galectin-1 (Gal-1). I, input; FT, flowthrough; B, bead-bound fraction. **F**.
958 PDAC087T cells were pre-treated with neuraminidase, then infected with H-1PV at an MOI of
959 250. Six hours post-infection, cells were fixed and stained with an antibody against the
960 conformational H-1PV capsid protein. Images were acquired using a confocal microscope with
961 a 63X objective, and fluorescence intensity was quantified. Data represent mean ± SD of three

962 independent experiments performed in triplicate. Statistical comparisons were performed using
963 an unpaired t test.

964 **Figure S4**. **A**. Western blot analysis of TGN46, galectin-1 (Gal-1), and laminin-γ1 expression
965 in the indicated PDAC-derived cell lines. GAPDH was used as a loading control. Data are
966 representative of three independent experiments. **B**. Western blot analysis of TGN46
967 expression in wild-type Panc-1 cells (non-targeting control) and Panc-1 cells expressing
968 *TGOLN2* sgRNA. GAPDH was used as a loading control. Data are representative of three
969 independent experiments. **C**. Immunofluorescence analysis of TGN46 expression in AsPC-1
970 cells either overexpressing (+) or not (–) TGN46. Data represent the mean ± SD of three
971 independent experiments, each performed in triplicate. Statistical comparisons were
972 performed using an unpaired t-test. **D**. Western blot analysis of TGN46 and galectin-1 (Gal-1)
973 expression in the indicated PDAC-derived primary cells. β-actin was used as a loading control.
974 Data are representative of three independent experiments.

975

976 **References**

977

978 1. Wood, L. D., Canto, M. I., Jaffee, E. M. & Simeone, D. M. Pancreatic Cancer: Pathogenesis,
979 Screening, Diagnosis, and Treatment. *Gastroenterology* **163**, 386-402.e1 (2022).
980 2. Park, W., Chawla, A. & O'Reilly, E. M. Pancreatic Cancer: A Review. *JAMA* **326**, 851–862 (2021).
981 3. Halbrook, C. J., Lyssiotis, C. A., Pasca di Magliano, M. & Maitra, A. Pancreatic cancer: Advances
982 and challenges. *Cell* **186**, 1729–1754 (2023).
983 4. Kollmann, C. F., van Montfoort, N., Cordelier, P., Pol, J. & Olagnier, D. Oncolytic virotherapy:
984 Sparking durable anti-tumor immunity through microenvironment modulation. *Semin Immunol*
985 **80**, 101994 (2025).
986 5. Zhang, T. *et al.* Talimogene Laherparepvec (T-VEC): A Review of the Recent Advances in Cancer
987 Therapy. *J Clin Med* **12**, 1098 (2023).
988 6. Quillien, L., Buscail, L. & Cordelier, P. Pancreatic Cancer Cell and Gene Biotherapies: Past,
989 Present, and Future. *Hum Gene Ther* **34**, 150–161 (2023).
990 7. Runcie, K. *et al.* Phase I study of intratumoral injection of talimogene laherparepvec for the
991 treatment of advanced pancreatic cancer. *Oncologist* oyae200 (2024)
992 doi:10.1093/oncolo/oyae200.
993 8. Angelova, A. L., Geletneky, K., Nüesch, J. P. F. & Rommelaere, J. Tumor Selectivity of Oncolytic
994 Parvoviruses: From in vitro and Animal Models to Cancer Patients. *Frontiers in Bioengineering*
995 *and Biotechnology* **3**, (2015).
996 9. Geletneky, K. *et al.* Oncolytic H-1 Parvovirus Shows Safety and Signs of Immunogenic Activity in a
997 First Phase I/IIa Glioblastoma Trial. *Molecular Therapy* **25**, 2620–2634 (2017).
998 10. Hajda, J. *et al.* A non-controlled, single arm, open label, phase II study of intravenous and
999 intratumoral administration of ParvOryx in patients with metastatic, inoperable pancreatic
1000 cancer: ParvOryx02 protocol. *BMC Cancer* **17**, 1–11 (2017).

1001 11. Hajda, J. *et al.* Phase 2 Trial of Oncolytic H-1 Parvovirus Therapy Shows Safety and Signs of
1002 Immune System Activation in Patients With Metastatic Pancreatic Ductal Adenocarcinoma.
1003 *Clinical Cancer Research* **27**, 5546–5556 (2021).
1004 12. Bretscher, C. & Marchini, A. H-1 Parvovirus as a Cancer-Killing Agent: Past, Present, and Future.
1005 *Viruses* **11**, 562 (2019).
1006 13. Hristov, G. *et al.* Through Its Nonstructural Protein NS1, Parvovirus H-1 Induces Apoptosis via
1007 Accumulation of Reactive Oxygen Species. *Journal of Virology* **84**, 5909–5922 (2010).
1008 14. Kulkarni, A. *et al.* Oncolytic H-1 parvovirus binds to sialic acid on laminins for cell attachment and
1009 entry. *Nat Commun* **12**, 3834 (2021).
1010 15. Ferreira, T. *et al.* Oncolytic H-1 Parvovirus Hijacks Galectin-1 to Enter Cancer Cells. *Viruses* **14**,
1011 1018 (2022).
1012 16. Vasta, G. R. Roles of galectins in infection. *Nat Rev Microbiol* **7**, 424–438 (2009).
1013 17. Ferreira, T. *et al.* Oncolytic H-1 Parvovirus Enters Cancer Cells through Clathrin-Mediated
1014 Endocytosis. *Viruses* **12**, 1199 (2020).
1015 18. Ferreira, T. *et al.* Oncolytic H-1 Parvovirus Enters Cancer Cells through Clathrin-Mediated
1016 Endocytosis. *Viruses* **12**, 1199 (2020).
1017 19. Toolan, H. W., Dalldore, G., Barclay, M., Chandra, S. & Moore, A. E. An unidentified, filtrable
1018 agent isolated from transplanted human tumors*. *Proceedings of the National Academy of*
1019 *Sciences* **46**, 1256–1258 (1960).
1020 20. Lujan, P. *et al.* Sorting of secretory proteins at the trans-Golgi network by TGN46. *eLife* **12**,
1021 (2023).
1022 21. Fraunhoffer, N. A. *et al.* Evidencing a Pancreatic Ductal Adenocarcinoma Subpopulation Sensitive
1023 to the Proteasome Inhibitor Carfilzomib. *Clin Cancer Res* **26**, 5506–5519 (2020).
1024 22. Angelova, A. L. *et al.* Complementary induction of immunogenic cell death by oncolytic
1025 parvovirus H-1PV and gemcitabine in pancreatic cancer. *J. Virol.* **88**, 5263–5276 (2014).

1026 23. Joung, J. *et al.* Genome-scale CRISPR-Cas9 knockout and transcriptional activation screening.
1027 *Nature Protocols* **12**, 828–863 (2017).
1028 24. Li, W. *et al.* MAGeCK enables robust identification of essential genes from genome-scale
1029 CRISPR/Cas9 knockout screens. *Genome Biology* **15**, 554 (2014).
1030 25. Agudelo, D. *et al.* Marker-free coselection for CRISPR-driven genome editing in human cells.
1031 *Nature Methods* **14**, 615–620 (2017).
1032 26. Tessmer, C. *et al.* Generation and Validation of Monoclonal Antibodies Suitable for Detecting and
1033 Monitoring Parvovirus Infections. *Pathogens* **11**, 208 (2022).
1034 27. Liu, X. *et al.* An AP-MS- and BioID-compatible MAC-tag enables comprehensive mapping of
1035 protein interactions and subcellular localizations. *Nat Commun* **9**, 1188 (2018).
1036 28. Zhuo, C. *et al.* Spatiotemporal control of CRISPR/Cas9 gene editing. *Signal Transduct Target Ther*
1037 **6**, 238 (2021).
1038 29. Li, J. *et al.* Synergistic combination of valproic acid and oncolytic parvovirus H-1PV as a potential
1039 therapy against cervical and pancreatic carcinomas. *EMBO Mol Med* **5**, 1537–1555 (2013).
1040 30. Mayle, K. M., Le, A. M. & Kamei, D. T. The intracellular trafficking pathway of transferrin. *Biochim*
1041 *Biophys Acta* **1820**, 264–281 (2012).
1042 31. Banting, G., Maile, R. & Roquemore, E. P. The steady state distribution of humTGN46 is not
1043 significantly altered in cells defective in clathrin-mediated endocytosis. *J Cell Sci* **111 (Pt 23)**,
1044 3451–3458 (1998).
1045 32. Schäfer, T. E. *et al.* Biomarker screen for efficacy of oncolytic virotherapy in patient-derived
1046 pancreatic cancer cultures. *EBioMedicine* **105**, 105219 (2024).
1047 33. Kulkarni, A. *et al.* Oncolytic H-1 parvovirus binds to sialic acid on laminins for cell attachment and
1048 entry. *Nat Commun* **12**, 3834 (2021).
1049 34. Paglino, J. C., Andres, W. & van den Pol, A. N. Autonomous parvoviruses neither stimulate nor
1050 are inhibited by the type I interferon response in human normal or cancer cells. *J Virol* **88**, 4932–
1051 4942 (2014).

1052 35. Neulinger-Muñoz, M. *et al.* Human Retrotransposons and the Global Shutdown of Homeostatic
1053 Innate Immunity by Oncolytic Parvovirus H-1PV in Pancreatic Cancer. *Viruses* **13**, 1019 (2021).
1054 36. Raykov, Z. *et al.* TLR-9 contributes to the antiviral innate immune sensing of rodent parvoviruses
1055 MVMp and H-1PV by normal human immune cells. *PLoS One* **8**, e55086 (2013).
1056 37. Lujan, P. *et al.* Sorting of secretory proteins at the trans-Golgi network by human TGN46. *eLife*
1057 **12**, RP91708 (2024).
1058 38. Wakana, Y. *et al.* Kinesin-5/Eg5 is important for transport of CARTS from the trans-Golgi network
1059 to the cell surface. *Journal of Cell Biology* **202**, 241–250 (2013).
1060 39. Wakana, Y. *et al.* A new class of carriers that transport selective cargo from the trans Golgi
1061 network to the cell surface. *The EMBO Journal* **31**, 3976–3990 (2012).
1062 40. Lee, M. *et al.* TGF-β-Induced PAUF Plays a Pivotal Role in the Migration and Invasion of Human
1063 Pancreatic Ductal Adenocarcinoma Cell Line Panc-1. *Int J Mol Sci* **25**, 11420 (2024).
1064 41. Kim, Y. J. *et al.* Pancreatic Adenocarcinoma Up-Regulated Factor (PAUF) Transforms Human
1065 Monocytes into Alternative M2 Macrophages with Immunosuppressive Action. *Int J Mol Sci* **25**,
1066 11545 (2024).
1067 42. Hutchison, J. M. *et al.* Recombinant SARS-CoV-2 envelope protein traffics to the trans-Golgi
1068 network following amphipol-mediated delivery into human cells. *J Biol Chem* **297**, 100940 (2021).
1069 43. Hatoyama, Y., Homma, Y., Hiragi, S. & Fukuda, M. Establishment and analysis of conditional
1070 Rab1- and Rab5-knockout cells using the auxin-inducible degron system. *J Cell Sci* **134**, jcs259184
1071 (2021).
1072 44. McLauchlan, H. *et al.* A novel role for Rab5-GDI in ligand sequestration into clathrin-coated pits.
1073 *Curr Biol* **8**, 34–45 (1998).
1074

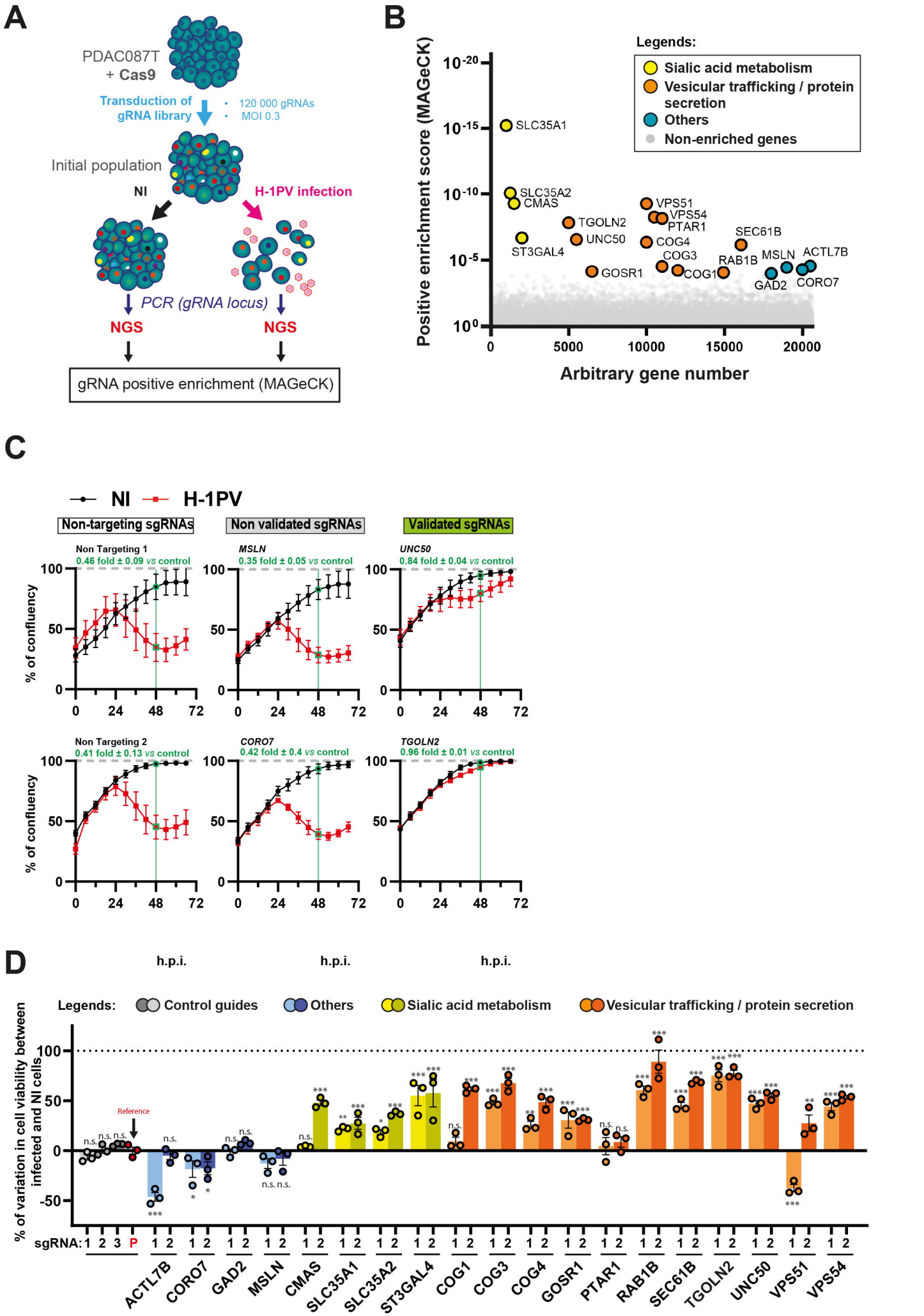
A
PDAC087T
+ Cas9
Transduction of
gRNA library
120 000 gRNAs
MOI 0.3
Initial population
NI
H-1PV infection
PCR (gRNA locus)
NGS
NGS
gRNA positive enrichment (MAGeCK)
B
Legends:
Sialic acid metabolism
Vesicular trafficking / protein secretion
Others
Non-enriched genes
Positive enrichment score (MAGeCK)
Arbitrary gene number
SLC35A1
SLC35A2
CMAS
ST3GAL4
TGOLN2
UNC50
GOSR1
VPS51
VPS54
PTAR1
COG4
COG3
COG1
SEC61B
RAB1B
MSLN
GAD2
ACTL7B
CORO7
C
NI
H-1PV
Non-targeting sgRNAs
Non validated sgRNAs
Validated sgRNAs
Non Targeting 1
0.46 fold ± 0.09 vs control
MSLN
0.35 fold ± 0.05 vs control
UNC50
0.84 fold ± 0.04 vs control
Non Targeting 2
0.41 fold ± 0.13 vs control
CORO7
0.42 fold ± 0.4 vs control
TGOLN2
0.96 fold ± 0.01 vs control
% of confluency
D
h.p.i.
Legends:
Control guides
Others
Sialic acid metabolism
Vesicular trafficking / protein secretion
% of variation in cell viability between infected and NI cells
Reference
sgRNA:
ACTL7B
CORO7
GAD2
MSLN
CMAS
SLC35A1
SLC35A2
ST3GAL4
COG1
COG3
COG4
GOSR1
PTAR1
RAB1B
SEC61B
TGOLN2
UNC50
VPS51
VPS54

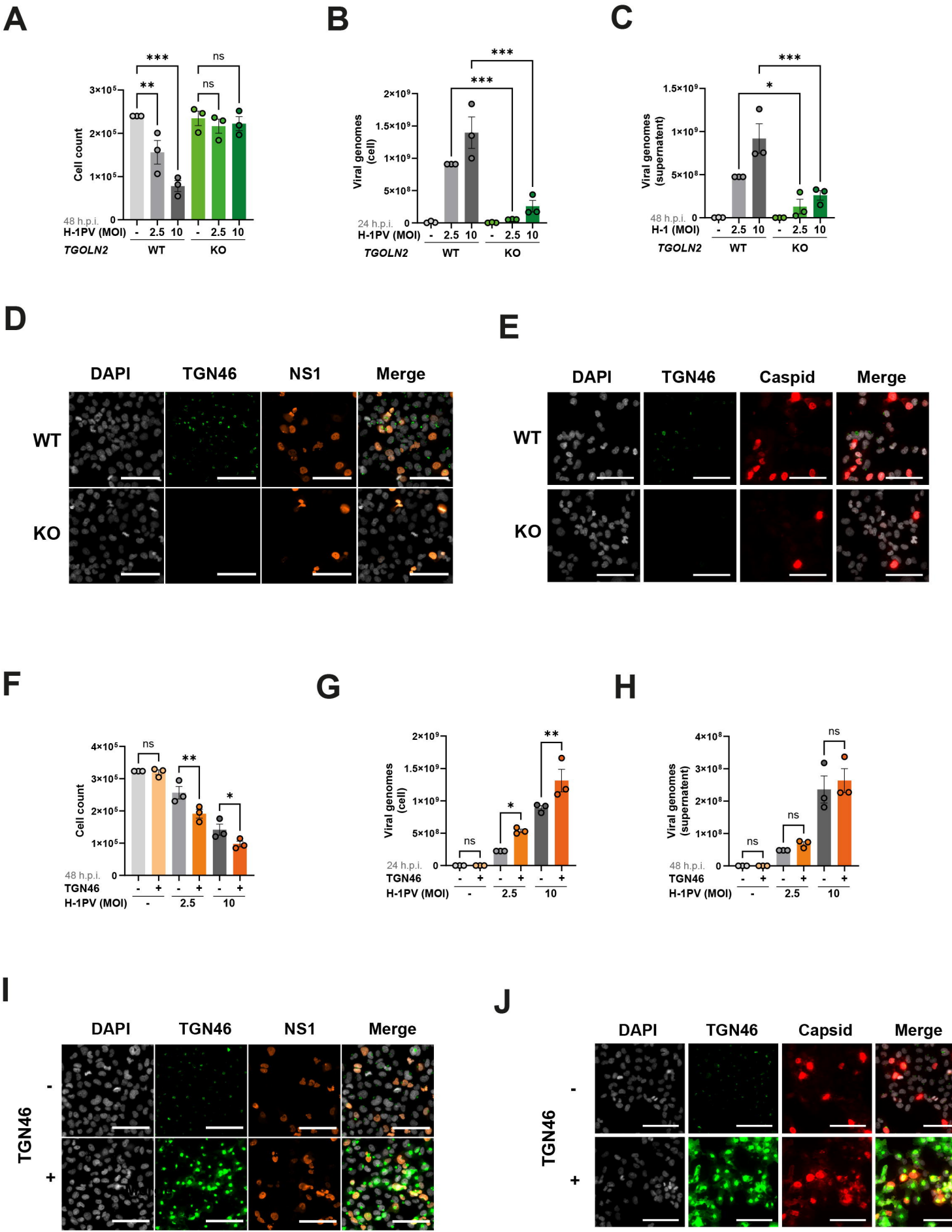
A
Cell count
3×10^5
2×10^5
1×10^5
0
48 h.p.i.
***
**
ns
ns
H-1PV (MOI)
-
2.5
10
-
2.5
10
TGOLN2
WT
KO
B
Viral genomes (cell)
2×10^9
1.5×10^9
1×10^9
5×10^8
0
24 h.p.i.
***
***
H-1PV (MOI)
-
2.5
10
-
2.5
10
TGOLN2
WT
KO
C
Viral genomes (supernatant)
1.5×10^9
1×10^9
5×10^8
0
48 h.p.i.
***
*
H-1 (MOI)
-
2.5
10
-
2.5
10
TGOLN2
WT
KO
D
DAPI
TGN46
NS1
Merge
WT
KO
E
DAPI
TGN46
Caspid
Merge
WT
KO
F
Cell count
4×10^5
3×10^5
2×10^5
1×10^5
0
48 h.p.i.
ns
**
*
TGN46
-
+
-
+
-
+
H-1PV (MOI)
-
2.5
10
G
Viral genomes (cell)
2×10^9
1.5×10^9
1×10^9
5×10^8
0
24 h.p.i.
ns
*
**
TGN46
-
+
-
+
-
+
H-1PV (MOI)
-
2.5
10
H
Viral genomes (supernatant)
4×10^8
3×10^8
2×10^8
1×10^8
0
48 h.p.i.
ns
ns
ns
TGN46
-
+
-
+
-
+
H-1PV (MOI)
-
2.5
10
I
DAPI
TGN46
NS1
Merge
TGN46
-
+
J
DAPI
TGN46
Capsid
Merge
TGN46
-
+

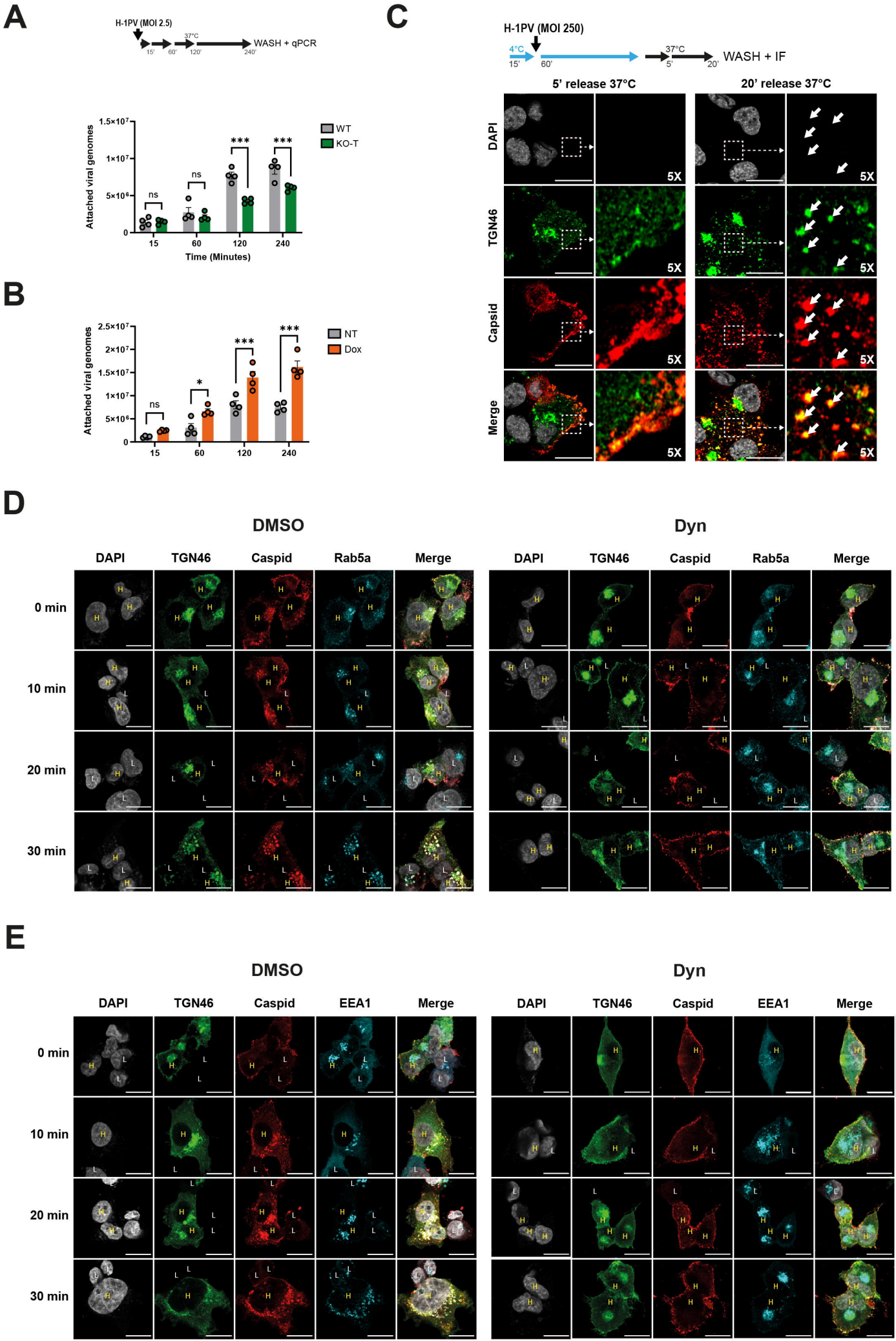
A
H-1PV (MOI 2.5)
15'
60'
37°C
120'
240'
WASH + qPCR
Attached viral genomes
1.5×10⁷
1×10⁷
5×10⁶
0
ns
ns
***
***
WT
KO-T
15
60
120
240
Time (Minutes)
B
Attached viral genomes
2.5×10⁷
2×10⁷
1.5×10⁷
1×10⁷
5×10⁶
0
ns
*
***
***
NT
Dox
15
60
120
240
C
H-1PV (MOI 250)
4°C
15'
60'
37°C
5'
20'
WASH + IF
5' release 37°C
20' release 37°C
DAPI
TGN46
Capsid
Merge
5X
D
DMSO
Dyn
DAPI
TGN46
Caspid
Rab5a
Merge
0 min
10 min
20 min
30 min
H
L
E
DMSO
Dyn
DAPI
TGN46
Caspid
EEA1
Merge
0 min
10 min
20 min
30 min
H
L

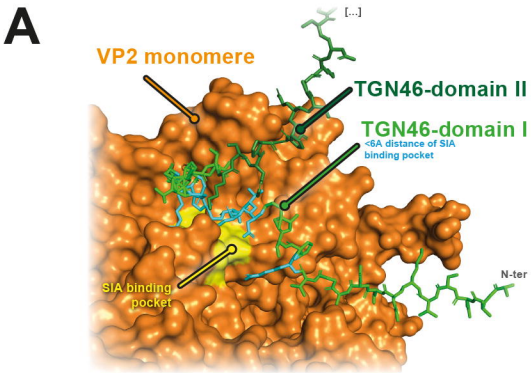
A
VP2 monomere
TGN46-domain II
TGN46-domain I
<6A distance of SIA binding pocket
SIA binding pocket
N-ter

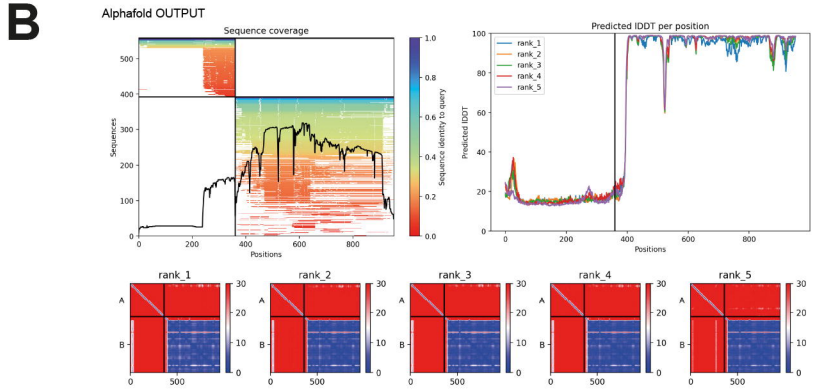
B
Alphafold OUTPUT
Sequence coverage
Sequences
Positions
Sequence identity to query
Predicted lDDT per position
Predicted lDDT
rank_1
rank_2
rank_3
rank_4
rank_5

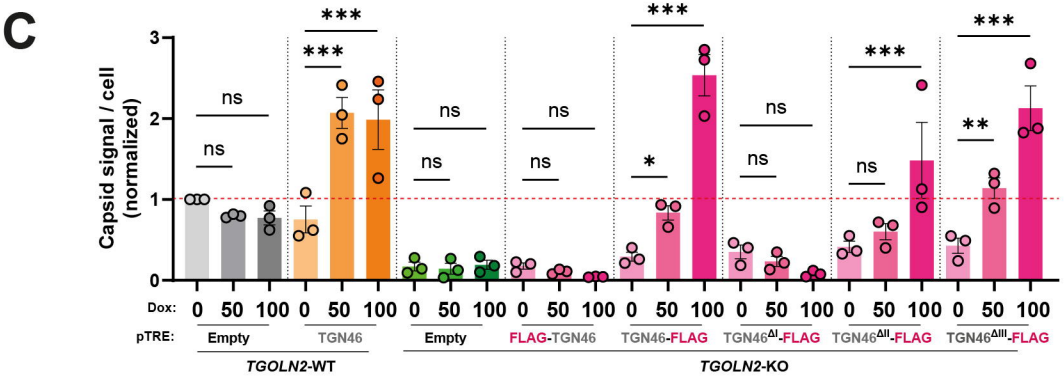
C
Capsid signal / cell (normalized)
Dox:
pTRE:
Empty
TGN46
FLAG-TGN46
TGN46-FLAG
TGN46ΔI-FLAG
TGN46ΔII-FLAG
TGN46ΔIII-FLAG
TGOLN2-WT
TGOLN2-KO
ns
*
**
***

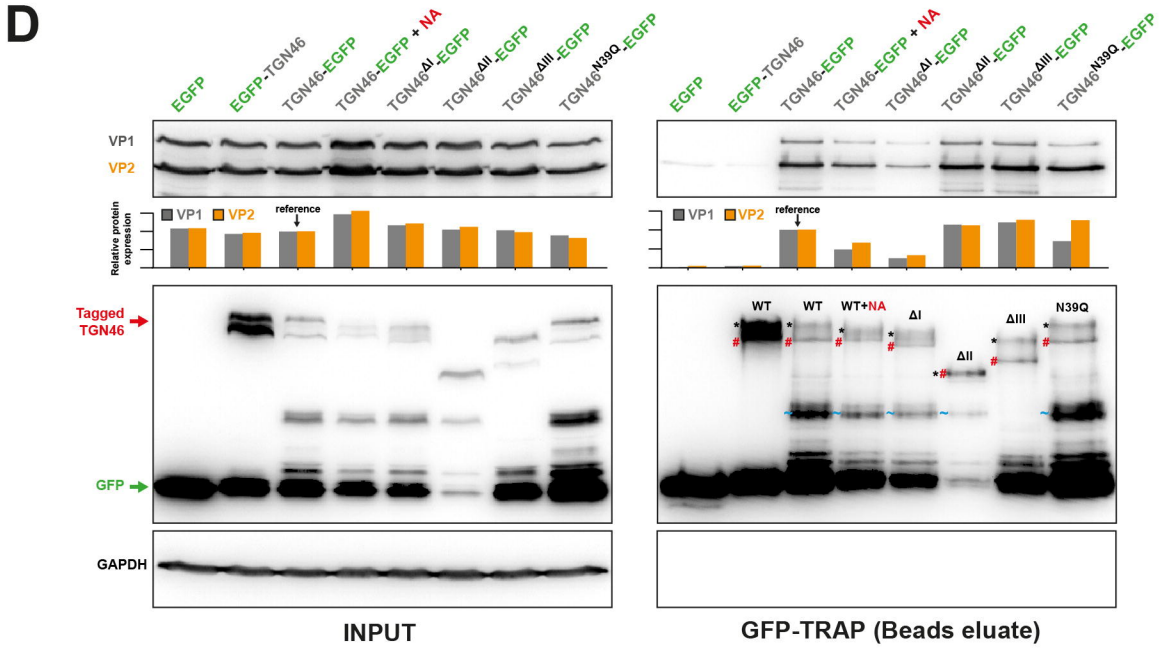
D
EGFP
EGFP-TGN46
TGN46-EGFP
TGN46-EGFP + NA
TGN46ΔI-EGFP
TGN46ΔII-EGFP
TGN46ΔIII-EGFP
TGN46N39Q-EGFP
VP1
VP2
Relative protein expression
reference
Tagged TGN46
GFP
GAPDH
WT
WT+NA
ΔI
ΔII
ΔIII
N39Q
INPUT
GFP-TRAP (Beads eluate)

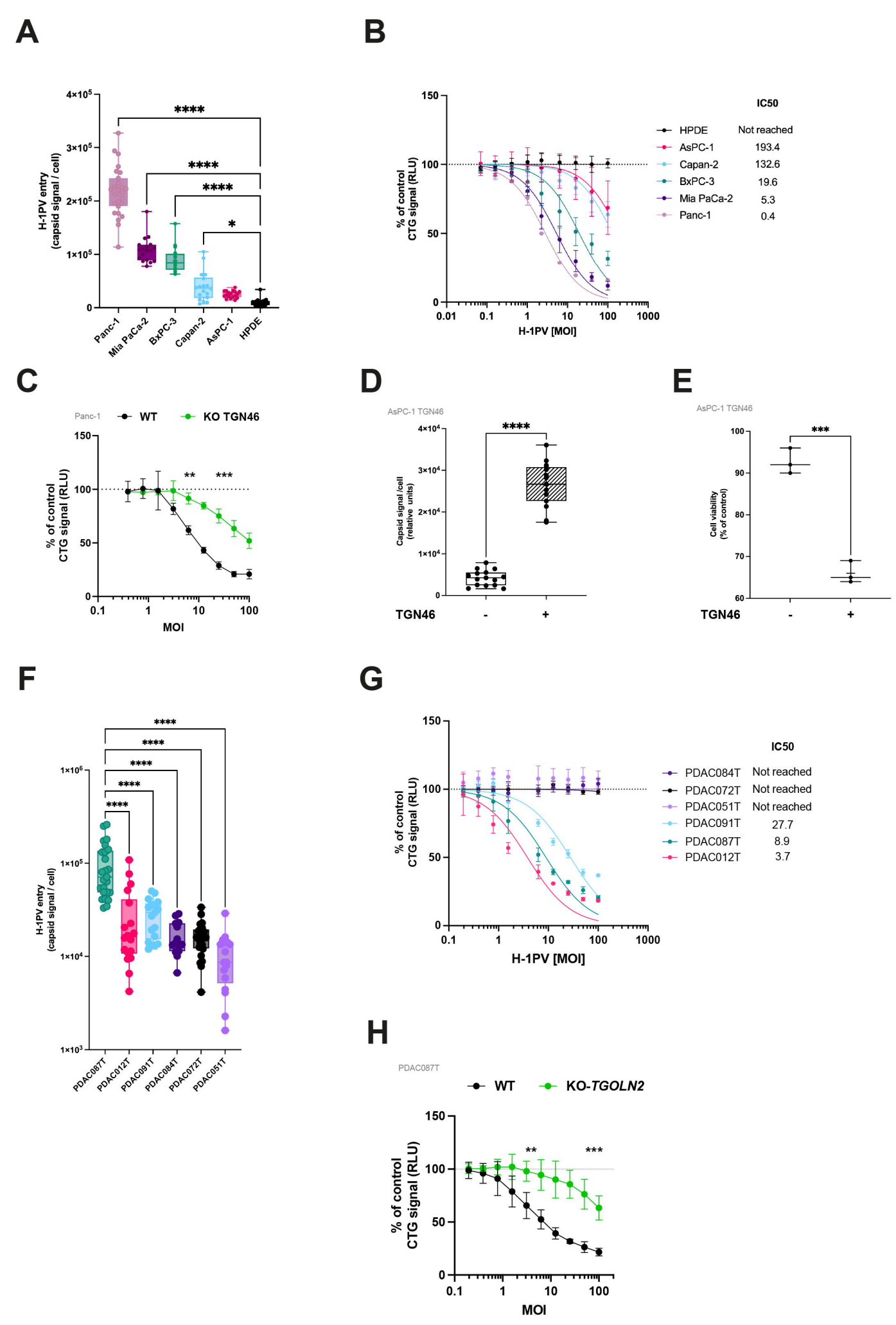
A
H-1PV entry (capsid signal / cell)
4×10^5
3×10^5
2×10^5
1×10^5
0
****
****
****
*
Panc-1
Mia PaCa-2
BxPC-3
Capan-2
AsPC-1
HPDE
B
% of control CTG signal (RLU)
150
100
50
0
0.01
0.1
1
10
100
1000
H-1PV [MOI]
IC50
HPDE Not reached
AsPC-1 193.4
Capan-2 132.6
BxPC-3 19.6
Mia PaCa-2 5.3
Panc-1 0.4
C
Panc-1
WT
KO TGN46
% of control CTG signal (RLU)
150
100
50
0
**
***
0.1
1
10
100
MOI
D
AsPC-1 TGN46
Capsid signal /cell (relative units)
4×10^4
3×10^4
2×10^4
1×10^4
0
****
TGN46
-
+
E
AsPC-1 TGN46
Cell viability (% of control)
100
90
80
70
60
***
TGN46
-
+
F
H-1PV entry (capsid signal / cell)
1×10^6
1×10^5
1×10^4
1×10^3
****
****
****
****
****
PDAC087T
PDAC012T
PDAC091T
PDAC084T
PDAC072T
PDAC051T
G
% of control CTG signal (RLU)
150
100
50
0
0.1
1
10
100
1000
H-1PV [MOI]
IC50
PDAC084T Not reached
PDAC072T Not reached
PDAC051T Not reached
PDAC091T 27.7
PDAC087T 8.9
PDAC012T 3.7
H
PDAC087T
WT
KO-TGOLN2
% of control CTG signal (RLU)
150
100
50
0
**
***
0.1
1
10
100
MOI

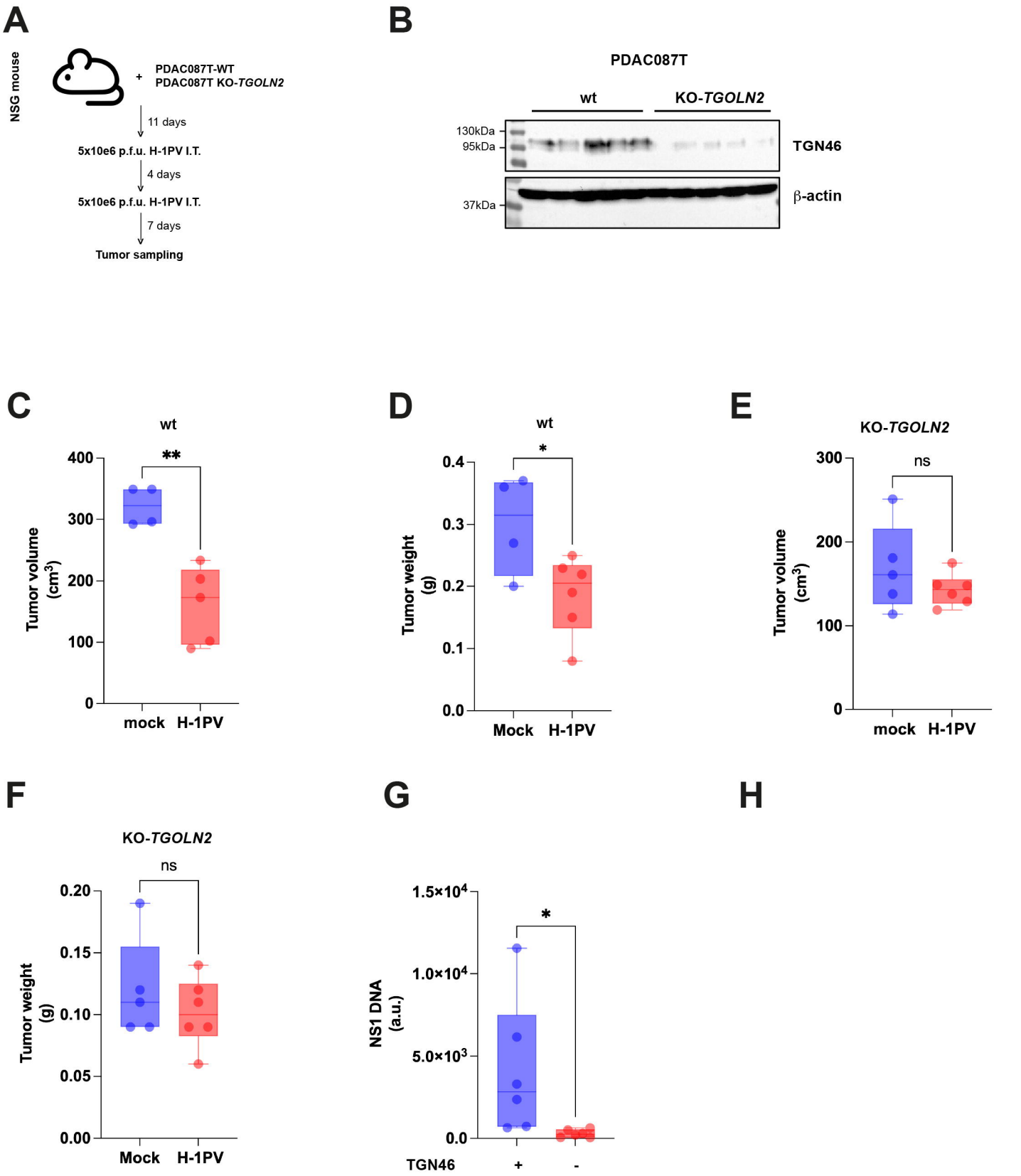
A
NSG mouse
+
PDAC087T-WT
PDAC087T KO-TGOLN2
11 days
5x10e6 p.f.u. H-1PV I.T.
4 days
5x10e6 p.f.u. H-1PV I.T.
7 days
Tumor sampling
B
PDAC087T
wt
KO-TGOLN2
130kDa
95kDa
TGN46
37kDa
β-actin
C
wt
**
Tumor volume (cm3)
400
300
200
100
0
mock
H-1PV
D
wt
*
Tumor weight (g)
0.4
0.3
0.2
0.1
0.0
Mock
H-1PV
E
KO-TGOLN2
ns
Tumor volume (cm3)
300
200
100
0
mock
H-1PV
F
KO-TGOLN2
ns
Tumor weight (g)
0.20
0.15
0.10
0.05
0.00
Mock
H-1PV
G
*
NS1 DNA (a.u.)
1.5×10^4
1.0×10^4
5.0×10^3
0.0
TGN46
+
-
H